MECHANICAL PROPERTIES IDENTIFICATION OF VISCOELASTIC / HYPERELASTIC MATERIALS BASED ON EXPERIMENTAL DATA

A THESIS SUBMITTED TO
THE GRADUATE SCHOOL OF NATURAL AND APPLIED SCIENCES
OF
MIDDLE EAST TECHNICAL UNIVERSITY

BY

ALİCAN TABAKCI

IN PARTIAL FULFILLMENT OF THE REQUIREMENTS
FOR
THE DEGREE OF MASTER OF SCIENCE
IN
MECHANICAL ENGINEERING

SEPTEMBER 2010

Approval of the thesis:

MECHANICAL PROPERTIES IDENTIFICATION OF VISCOELASTIC / HYPERELASTIC MATERIALS BASED ON EXPERIMENTAL DATA

submitted by **ALİCAN TABAKCI** in partial fulfillment of the requirements for the degree of **Master of Science in Mechanical Engineering Department, Middle East Technical University** by,

Prof. Dr. Canan Özgen
Dean, Graduate School of **Natural and Applied Sciences** _____

Prof. Dr. Süha Oral
Head of Department, **Mechanical Engineering** _____

Asst. Prof. Dr. E. İlhan Konukseven
Supervisor, **Mechanical Engineering Dept., METU** _____

Prof. Dr. Aydan Erkmen
Co-Supervisor, **Electrical and Electronics Engineering Dept., METU** _____

Examining Committee Members:

Prof. Dr. Tuna Balkan
Mechanical Engineering Dept., METU _____

Asst. Prof. Dr. İlhan Konukseven
Mechanical Engineering Dept., METU _____

Prof. Dr. Aydan Erkmen
Electrical and Electronics Engineering Dept., METU _____

Asst. Prof. Dr. Ergin Tönük
Mechanical Engineering Dept., METU _____

Asst. Prof. Dr. Buğra Koku
Mechanical Engineering Dept., METU _____

Date: 24.09.2010

I hereby declare that all information in this document has been obtained and presented in accordance with academic rules and ethical conduct. I also declare that, as required by these rules and conduct, I have fully cited and referenced all material and results that are not original to this work.

Name, Last name: Alican Tabakcı

Signature:

ABSTRACT

MECHANICAL PROPERTIES IDENTIFICATION OF
VISCOELASTIC / HYPERELASTIC MATERIALS
BASED ON EXPERIMENTAL DATA

Tabakcı, Alican
M.S., Department of Mechanical Engineering
Supervisor: Asst. Prof. Dr. E. İlhan Konukseven
Co-Supervisor: Prof. Dr. Aydan Erkmen

September 2010, 118 pages

Mechanical simulation of viscoelastic materials and assigning a viscoelastic material to the modeled parts in the simulations are difficult task. For the simulations, material model should be well chosen and material coefficients of the chosen models should be known.

In order to obtain accurate simulations, hyperelastic characteristics of the viscoelastic materials should be investigated and hyperelastic model should be incorporated in the solutions. Material models and material model's coefficients are chosen with the help of mechanical tests/experiments for these situations.

The main goal of this thesis is to optimize material model's coefficients by using an indenter test setup results and inverse finite element modeling. To achieve this, firstly by using a haptic device and other required equipments an indenter setup was prepared to test the materials mechanically. Inverse finite element modeling method is used in order to model the materials according to their viscoelastic and

hyperelastic characteristics. The model obtained from analysis was optimized by using the results obtained from indenter setup according to experimental test data. By doing this, the correctness of the model chosen by inverse finite element modeling was proved for the tested material and material model coefficients were calculated correctly.

Keywords: viscoelastic, hyperelastic, inverse finite element, indenter test setup

ÖZ

DENEYSEL DATAYA DAYALI VİSKOELASTİK / HİPERELASTİK MALZEMELERİN MEKANİK ÖZELLİKLERİNİN TANIMLANMASI

Tabakcı, Alican
Yüksek Lisans, Makine Mühendisliği Bölümü
Tez Yöneticisi: Yar. Doç. Dr. E. İlhan Konukseven
Ortak Tez Yöneticisi: Prof. Dr. Aydan Erkmen

Eylül 2010, 118 sayfa

Viskoelastik yapıya sahip malzemelerin bilgisayar ortamında mekanik özelliklerinin belirlenmesi ve modellenen parçaya viskoelastik malzeme modeli atayarak simulasyonu zordur. Bu tür durumlarda simulasyonu yapılcak olan malzemenin, malzeme modelinin uygun seçilmesi ve seçilen modellerin malzeme katsayılarının bilinmesi gerekir.

Daha gerçekçi simulasyon için genellikle viskoelastik malzemenin hiperelastik yapısıda incelenir ve hiperelastik modeli de yapılan çözümlere dahil edilir. Bu işlem için dışardan mekanik bir malzeme testi/deneyi yapılarak, alınan verilerin yardımı ile malzeme modelleri ve katsayıları seçilir.

Bu tezin ana amacı, viskoelastik yapılı bir malzemenin indentör test düzeneği yardımıyla evrik sonlu elemanlar yönteminde modellenmesi ve kullanılan modeller için malzeme katsayılarının yapılan deneylere göre optimizasyonudur.

Bu tezde ilk olarak, mekanik malzeme testleri/deneyleri için haptik cihaz ve gerekli olan diğer ekipmanlar kullanarak indentör deney sistemi kurulmuştur.

Evrik sonlu elemanlar yöntemiyle ve seçilen ilk malzeme model katsayılarana göre, test edilen malzemeler viskoelastik ve hiperelastik yapılarıyla modellenmiştir. Analizden çıkan model katsayıları indentör deney sisteminden gelen sonuçlar yardımıyla yapılan deneyin özelliklerine göre optimize edilmiştir. Bu sayede test yapılan malzeme için, evrik sonu elemanlar yönteminde seçilen modelin doğruluğu kanıtlanmış ve modellerdeki gerekli olan malzeme katsayıları yapılan deneylere göre hesaplanmıştır.

Anahtar Kelimeler : viskoelastik, hiperelastik, evrik sonlu elemanlar, indentör deney düzeneği

ACKNOWLEDGEMENTS

First, I would like to express my gratitude to my Supervisor Asst. Prof. Dr. E. İlhan Konukseven and co-supervisor Prof. Dr. Aydan Erkmen for their supervision, guidance, support and encouragement during the study. Without their knowledge and support I would not complete this study.

I would like to express my sincere thanks to Muran Bilen and his engine software for help in my thesis.

I would like to thank Tekfalt Makina and all employees for their great support.

I am grateful to all the stuff of the Department of Mechanical Engineering. I must thank my dear lab mates Gökhan Bayar, Özgür Başer, Serter Yılmaz and Berk Yurttagül for their supports and also for their friendships.

I must also express my special thanks to Ali Erdem Eken, Görkem Demircioğlu, Erdem Erişen and Mete Han Hocaoğlu for being always there for me.

Finally I want to express my great thanks to my family who gave their endless love and support during my life. I am thankful to my mother, father and sister, Gürsel, Ender and Merve Tabakcı.

TABLE OF CONTENTS

ABSTRACT iv
ÖZ vi
ACKNOWLEGMENTS viii
TABLE OF CONTENTS ix
LIST OF FIGURES xii
LIST OF TABLES xv

CHAPTERS
1. INTRODUCTION 1
2. LITERATURE SURVEY 7
2.1 Definition of Viscoelasticity 7
2.1.1 Properties of Viscoelastic Materials 8
2.1.1.1 Creep 8
2.1.1.2 Stress Relaxation 9
2.1.1.3 Hysteresis 10
2.1.2 Viscoelastic Material Modeling 10
2.1.2.1 Maxwell Model 11
2.1.2.2 Kelvin-Voigt Model 12
2.1.2.3 Standard Linear Model 13
2.1.2.4 Generalized Maxwell Model 13
2.1.3 Example Model of Viscoelasticity 14
2.1.3.1 Soft Tissue Modeling 14
2.1.3.2 Mechanical Properties of Soft Tissue 15
2.1.4 Material Test Methods for Soft Tissue 16
2.1.5 Device Used in Soft Tissue Test 17

2.1.5.1 Indenter Tests 17
2.2 Definition of Elasticity and Hyperelasticity 18
2.2.1 Hyperelastic Materials 20
2.2.2 Properties of Hyperelastic Materials 21
2.2.3 Hyperelastic Material Modeling 22
2.3 Previous Studies 22
3. EXPERIMENTAL SETUP 26
3.1 Problem Characteristics 26
3.2 Requirements for the Experimental Setup 27
3.3 Experimental Setup 28
3.3.1 Haptic Device 28
3.3.2 Force Sensor and Data Acquisition Card 30
3.3.3 Manufactured Materials 32
3.3.4 Controller Interface and GUI 34
4. FINITE ELEMENT ANALYSIS 42
4.1 Introduction 42
4.2 Material Nonlinearity and Nonlinear Analysis 43
4.3 Large Deformation 47
4.4 Structure of the Finite Element Model in ANSYS 48
4.4.1 Model 48
4.4.2 Geometry and Material Selection 49
4.4.3 Hyperelastic Material Finite Model for Tested Material Model 50
4.4.3.1 Ogden Model 54
4.4.3.2 The Polynomial Form 55
4.4.3.3 Two Term Mooney-Rivlin Model 56
4.4.4 Viscoelastic Material Finite Model for Tested Material Model 56
4.4.4.1 Constitutive Equations 57
4.4.5 Contact and Friction 60
4.4.5.1 Theory of Contact in ANSYS 61

4.4.5.2 Thermal Conductance 65
4.4.5.3 Offsets 66
4.4.5.4 Pinball Region 66
4.4.6 Meshes 67
4.5 Flexible Dynamic Analysis 70
4.6 Commands 76
5. OPTIMIZATION 84
5.1 Design of Experiments 86
5.2 Structure of DesignXplorer 87
5.2.1 Parameters 87
5.2.2 Automatic Design Points 88
5.2.3 Responses 89
5.2.4 Goal Driven Optimization 89
6. RESULTS 93
6.1 Inverse Finite Element Solution with Initial Values 94
6.2 Experiment Results 97
6.3 Optimization Results 98
6.3.1 Material Coefficients 99
6.3.2 3D Graphs of Material Coefficients Respect to RF Parameters 100
6.4 Inverse Finite Element Solution with Optimized Values 105
6.5 Comparison of Results 108
6.6 Optimization Results of Other Materials 109
7. CONCLUSION 112
REFERENCES 116

LIST OF FIGURES

FIGURES

Figure 2.1 Strain as a function of time due to constant stress over an extended period for a viscoelastic material [3] 9
Figure 2.2 Applied strain (a) and induced stress (b) as functions of time for a viscoelastic material [3] 9
Figure 2.3 Stress-Strain Curves for a purely elastic material (a) and a viscoelastic material (b). The shaded area is a hysteresis loop and shows the amount of energy lost (as heat) in a loading and unloading cycle [3] 10
Figure 2.4 Models of Linear Viscoelasticity: (a) Maxwell Model (b) Voigt Model (c) Kelvin Model [10] 11
Figure 2.5 The skin layers [15] 15
Figure 2.6 Load-Extension Curve & Influence of the train rate [16] 16
Figure 2.7 Indenter device loading representation [19] 18
Figure 2.8 Stress-strain curve of a linear elastic material [20] 20
Figure 3.1 Experimental Setup 27
Figure 3.2 Phantom Premium Haptic Device 29
Figure 3.3 Force Sensor Calibration 31
Figure 3.4 Force Sensor Adaptor and Probe 33
Figure 3.5 Manufactured Chassis 34
Figure 3.6 Controller Interface 35
Figure 3.7 PID Menu 36
Figure 3.8 Block Diagram of PID 37
Figure 3.9 Path Menu 38
Figure 3.10 Data Acquisition Menu 39
Figure 3.11 Analyses Menu 40

Figure 4.1 Stress strain relationship causing Material Nonlinearity [23] 44
Figure 4.2 Contact Nonlinearity [23] 44
Figure 4.3 Nonlinearity between load and response [23] 45
Figure 4.4 Newton-Raphson Method [23] 46
Figure 4.5 Model Tree of ANSYS 49
Figure 4.6 Contact Region [24] 61
Figure 4.7 Penetration [24] 62
Figure 4.8 Iteration [24] 63
Figure 4.9 Chattering 64
Figure 4.10 Different Types of Meshes [2] 67
Figure 4.11 Meshes 68
Figure 4.12 Time Steps 74
Figure 4.13 Force Reaction Graph 75
Figure 5.1 APDL Parameters 85
Figure 5.2 Structure of DesignXplorer 87
Figure 5.3 Goal Driven Optimization 90
Figure 5.4 Sample Points Generated by Screening Method 91
Figure 5.5 3-D Plots with Solution Points 92
Figure 6.1 Penetration Graph and Simulation for Initial Values 95
Figure 6.2 Equivalent Stress Graph and Simulation for Initial Values 95
Figure 6.3 Equivalent Elastic Strain Graph and Simulation for Initial Values 96
Figure 6.4 Maximum Principal Elastic Strain Graph and Simulation for Initial Values 96
Figure 6.5 Force Reaction (Relaxation) Graph for Initial Values 97
Figure 6.6 Filtered Smooth Experimental Data 98
Figure 6.7 Input Parameters and Candidate (optimized) Parameters Taken from ANSYS 98
Figure 6.8 C10 and C01 Coefficients Respect to RF 101
Figure 6.9 T1 and T2 Coefficients Respect to RF 102
Figure 6.10 A1 and A2 Coefficients Respect to RF 103
Figure 6.11 T1 and A1 Coefficients Respect to RF 104

Figure 6.12 T2 and A2 Coefficients Respect to RF 104
Figure 6.13 Penetration Graph and Simulation for Optimized Values 105
Figure 6.14 Equivalent Stress Graph and Simulation for Optimized Values 106
Figure 6.15 Equivalent Elastic Strain Graph and Simulation for Optimized Values 106
Figure 6.16 Maximum Principal Elastic Strain Graph and Simulation for Optimized Values 107
Figure 6.17 Force Reaction (Relaxation) Graph for Optimized Values 107
Figure 6.18 Optimization Result 108
Figure 6.19 Optimization Result for Viscoelastic Foam w/ 6 mm 109
Figure 6.20 Optimization Result for Viscoelastic Foam w/ 8 mm 110
Figure 6.21 Optimization Result for Soft Tissue (Arm) w/ 8 mm 110

LIST OF TABLES

TABLES

Table 2.1 The Mooney-Rivlin Coefficients 24
Table 4.1 Units of experimental conditions 48
Table 4.2 Comparison of Penalty Method and Lagrange Method 65
Table 6.1 Material Coefficients 99

CHAPTER 1

INTRODUCTION

The ultimate goal in this study is to identify in vivo soft tissue material characteristics such as human skin sampled on the face or on the arm. Human skin has been demonstrated to possess the following viscoelastic properties: stress relaxation, hysteresis and creep. When a soft tissue is suddenly extended and maintained at its new length, the stress gradually decreases slowly due to the stress relaxation. Creep is another property, when the soft tissue suddenly loaded with a constant tension, its lengthening velocity decrease against time until equilibrium. Additionally, under cyclic loading, the stress-strain curve shows two distinct paths corresponding to the loading and unloading trajectories; this property is called hysteresis. Identification of soft tissue is very difficult because of the contributions of these constituents to the overall mechanical behavior. Constituents' ratio is changing in every different part of human body. And also other identification difficulty is coming from mechanical properties of soft tissue. Soft tissues are clearly quasi-incompressible, non-homogeneous, non isotropic and non-linear viscoelastic materials in large deformation.

In order to achieve this ultimate goal, where the inherent complexities of the problem have been aforementioned, one must go through the following milestones. First, a new haptic device with proper loading capacity can be designed to make required indenter movements such as penetration and torsion. This device and its mounted force sensors may work in several axes with respect to high counter forces.

By this way, a user may obtain different material properties using special design experimental setup.

Material properties are changing due to structure of material and different material properties can be seen in different areas/sections of the same material. Soft tissues are a good example for that kind of material; its mechanical properties may change from one region to another. In order to model the mechanical behavior of the different regions of a multimodal material, experiments must be repeated for these regions. The point contact simulation can be enlarged to multimodal material simulation considering the smooth transitions between the regions with different material properties. Besides, with the help of special design experimental setup user can make different experiments (stress relaxation test, creep test, torsion test etc.) and may get proper data for required point contact modeling procedures.

Generally correct model of a material can only be achieved by properly identifying the mechanical properties of this material. Since a generic in vivo soft tissue modeling does not exist, the main objective of this thesis is to identify the stress relaxation characteristic of soft tissue and soft tissue like materials such as viscoelastic foam/gel. Towards this objective, we first developed a testing apparatus versatile for soft tissue stress relaxation testing. We chose the upper arm close to elbow as a human skin and artificial viscoelastic foam and gel as the testing materials. These materials are viscoelastic materials and suitable for our experimental setup.

The simulation environment used for model justification is chosen as a finite analysis tool. By using such a modeling procedure, simulation and optimization processes of the tested material can be performed simultaneously in software.

Most of the drawing or analyzing software's (CAD Software's, Finite Element Analysis Software etc.) used by engineers in daily life does not support an option to assign/designate a viscoelastic material feature to a selected body. This lack of

feature forces users to search and implement different algorithms as outsourced patches, which are not in the original software package.

Consequently in this thesis we developed an algorithm to express viscoelastic behavior in finite element analyses. A special algorithm was created and a new model simulated to solve this problem. Also, this model must be valid for selected hyperelastic model from library.

Viscoelastic models exist in the literature with undefined coefficients. This model can be generalized for all viscoelastic or viscoelastic like behavior in natural or manufactured materials. Consequently, material identification based upon a model can be justified by simulation. According to experimental test results on our selected material samples a model is selected in order to identify the material characteristics and the coefficients.

Material identification should be based on model justification. Since our objective is justification through simulation, it is necessity to correct any errors or inaccuracies, if any, between the simulated model and the real life example based on their subsequent comparisons. The use of optimization or any other known method to improve the results and correct the errors is the next step of the proposed process. As a result of these steps, it can be concluded that the tested material is adequately modeled based on the selected experimental method.

Modeling an in-vivo human skin sample not only encompasses viscoelastic behavior but also includes higher level elasticity together with hyperelastic characteristics in identification in order to increase modeling accuracy and decrease modeling errors in justification. During the optimization process, along with viscoelastic coefficients, hyperelastic model coefficients help the users to get more accurate and closer results for material modeling. With the use of both structures and their application methods in the computer simulated models, the margin of error gets lower and the results get closer to the real examples.

In order to achieve a proper and successful simulation of viscoelastic materials in terms of finite element analysis, complex algorithms have to be applied, since the materials show non-linear characteristics. For example, in case of soft organ tissues, the variables at consideration are very complex non-linear, anisotropic, non-homogeneous [1].

Besides the models need to be analyzed not only for their non-linearity characteristic, but also for their time dependency. In case of time in finite element analysis, a transient excitation is a highly dynamic, time-dependent force exerted on the model or structure, such as impacts and penetrations [2]. The deformation in the material depends on the load it is exposed to. Furthermore, this deformation can only be observed and analyzed within short time intervals. In the end, each analysis has to be in compliance with the subsequent time interval, like for a harmonic structure. Time and rate dependent behaviors of the material makes the measurement and simulation processes extremely challenging. As a combination, the geometric, material and contact non-linearity characteristics compose a much more complex structure, hence making the model analysis a harder job to complete.

In light of the examples given above, it can be easily observed that in order to achieve a proper simulation in a computer environment, very careful and precise experiments have to be completed. The resulting data for these experiments have to be properly filtered, so that they can be used in the finite element analysis. During this analysis, the filtered data is used in the analysis as compliance with the models of the materials at hand, and such data is also required for further optimization.

Satisfying all these requirements can only be possible if a versatile experimental setup is used for viscoelastic materials identification. As a result of this experimental setup and finite element analysis, with the help of cross-checking algorithms, we aimed to increase the accuracy of the stress relaxation experiments. Consequently, the coefficients of the identified and modeled material are properly justified based on modeled versus real behavior comparisons.

The major milestones of our work begin by selection of suitable material model based on determining model coefficients using correct material test method. The other milestone of our identification approach is to optimize material coefficients using material test data.

The methodology of this thesis can be summed up in three main issues handled:

The first major part of our approach focuses on modeling initial conditions on ANSYS, together with the identification of suitability of selected models based on their initial material coefficients with finite elements analysis method. The selected models (Mooney Rivlin model and Prony Series) are suitable for characterizing hyperelastic and viscoelastic behavior in finite element analysis simulation. The model stress relaxation data can be taken from ANSYS. After that, model's coefficients are optimized in ANSYS by using their stress relaxation data. During this process, all characteristics of viscoelastic structure (non-linearity, time dependency, time transient etc.) are carefully added to the simulation, hence giving time dependent and flexible dynamic results. So, stress relaxation test is simulated in real time using ANSYS.

The second part sets the requirements in experimental setup design for the necessary tests to be conducted. A haptic device is chosen as an indenter test setup, as a universal versatile tool for testing artificial materials samples as well as skin parts of the human body. Stress relaxation tests are selected to be conducted using this experimental setup. Moreover, this test method can be simulated using ANSYS, so that simulated data and tested data can be compared/used for optimization process.

The third, and the last, part mainly concentrates on the optimization of a model, which is tested and analyzed with initial stress relaxation data in compliance with stress relaxation test data. As a result a new model has been developed with

optimized material coefficients and the data from this model analysis is compared with the experimental data.

The task developed for soft tissue identification which lay in the objective of this work has brought two major contributions. An indenter test setup prepared to perform stress relaxation tests has been developed by modifying haptic device. Using this interface; a user can realize other material tests such as static and cyclic loading and creep test. The movement of indenter is directly controllable from computer and possesses the flexibility to move in its working area. A user can perform various tests for the other soft viscoelastic materials such as rubber and elastic gel by tuning PID parameters.

The second contribution lies in the optimization of model coefficients using ANSYS. Moreover our optimization architecture enables the user to be able to optimize other suitable viscoelastic materials coefficients using stress relaxation data.

Outline of this thesis is given as follows. After giving introduction, the detailed literature survey is presented in Chapter 2. The experimental setup and its properties are expressed in Chapter 3. The developed controller and its graphical user interface are also given in this chapter. Finite element analysis method and the specifications of the simulated models are expressed in Chapter 4. Optimization process, which is performed by using related ANYSY tools, is represented in Chapter 5. All the results, graphs and the comparisons are given in detailed in the result section, Chapter 6. The last section is related to the conclusion of this study.

CHAPTER 2

LITERATURE SURVEY

In order to simulate of viscoelastic materials on finite element analysis, the first step is selecting models and their initial material coefficients by using proper finite elements analysis method. In this study, selected models (Mooney Rivlin model and Prony Series) are suitable for the characterization of the hyperelastic and viscoelastic behaviors in finite element analysis simulation. Therefore, model's stress relaxation data can be obtained from finite element software. During this process, all characteristics of viscoelastic structures (non-linearity, time dependency, time transient etc.) are considered in the simulation.

2.1 Definitions of Viscoelasticity

Elastic materials hold Hooke's Law that, the stress is proportional to the strain. However for a purely viscous material, stress is the function of rate of strain, and this function known as viscosity [6]. Elasticity is usually the result of bond stretching along crystallographic planes in an ordered solid but viscosity is the result of the diffusion of atoms or molecules inside an amorphous material [7]. Materials that fall into neither classification mentioned are called viscoelastic materials.

In viscoelastic materials, upon loading, firstly an elastic response is monitored and then slow continual change in the response at a descending rate can be observed.

For a viscoelastic material the rate of stressing affects the time-dependent response of the material. For example, the larger the related strain, the longer it takes to reach the final value of stress at a constant rate of stressing. That is, viscoelastic materials possess a memory that keeps a record of their response history. This memory effect is evident in the constitutive relationship between the stress and strain tensors [6]

A viscoelastic material has the following properties: creep, stress relaxation and hysteresis.

2.1.1 Properties of Viscoelastic Materials

2.1.1.1 Creep

Creep is the deformation of a solid material perennially or propensity to slowly move under the influence of stresses [8]. Exposure to high levels of stress below the yield strength of the material cause creep effect. There are three stages for creep characteristics of a viscoelastic material [7].

- First stage (primary creep): The strain rate is relatively high but decelerates with increasing strain.
- Second stage (steady-state creep): Upon reaching its final state, the strain rate gets to its minimum value, which is nearly a constant value. The term Creep Strain Rate is derived from this second stage. The rate of stress and its dependence rate are in compliance with the creep mechanism.
- Third stage (tertiary creep): the strain rate exponentially increases with strain because of necking phenomena.

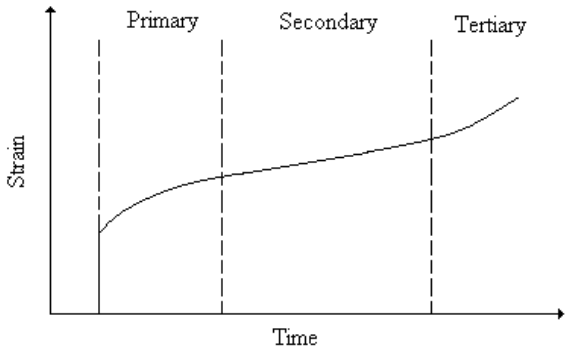

Figure 2.1 Strain as a function of time due to constant stress over an extended period for a viscoelastic material. [3]

2.1.1.2 Stress Relaxation

Stress relaxation is the decrease in stress over time when a material is prolonged to a previously set length. Creep and stress relaxation are nonlinear responses and have important implications for stretching and risk of injury in repetitive tasks [9].

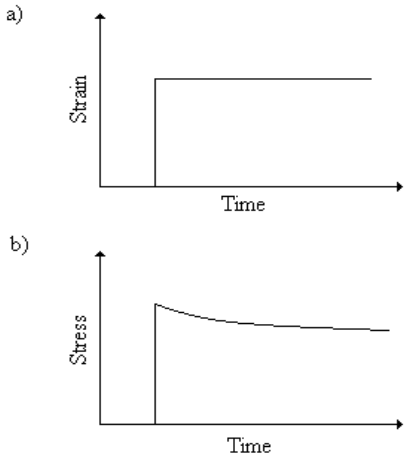

Figure 2.2 Applied strain (a) and induced stress (b) as functions of time for a viscoelastic material. [3]

2.1.1.3 Hysteresis

Hysteresis is the property of viscoelastic materials of having a different unloading response, when compared with their loading response (Figure 2.3). Hysteresis also provides a measure of the amount of energy lost because the material is not perfectly elastic [7].

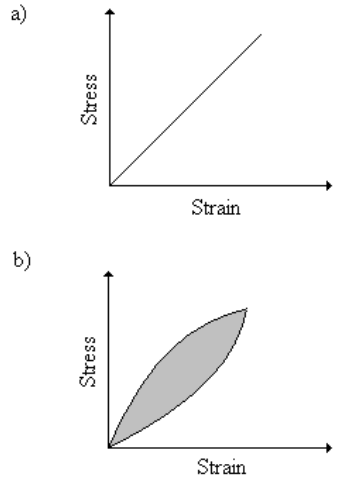

Figure 2.3 Stress-Strain Curves for a purely elastic material (a) and a viscoelastic material (b). The shaded area is a hysteresis loop and shows the amount of energy lost (as heat) in a loading and unloading cycle. [3]

2.1.2 Viscoelastic Material Modeling

Nearly all of the structural metals act as linear elastic when they are exposed to small strain. Although this does not count as a valid proof, the characteristic of a material is linear elastic when simple harmonic free vibrations exist in time. Moreover, the vibration of metals do not last forever even in a vacuumed place. It shows that metals sometimes leave Hooke's law. So, there have to be different laws in usage. When organic polymers are taken into account, the need for that extension is revealed.

Time is another important parameter for linear relationship in simple class of materials. Viscoelastic materials keep linearity between load and deflection due to time and also, without knowing the whole situation of loading, one cannot designate the present situation of deformation.

Most of the materials have a good memory to remember, compared with a linear elastic solid. It has a simple one and remembers just only the unstrained natural state. However, the other materials record their past situations. Material with memory means that they remember their previous state.

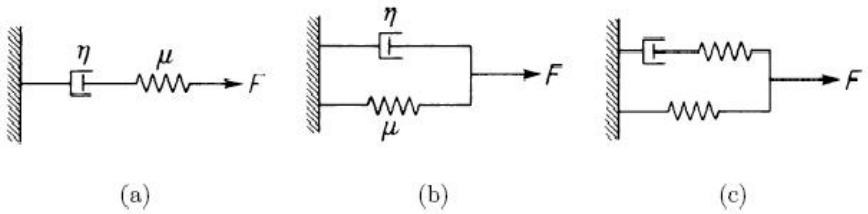

Figure 2.4 Models of Linear Viscoelasticity: (a) Maxwell Model (b) Voigt Model (c) Kelvin Model [10]

Let us consider some simple models in viscoelasticity. Figure 2.4 shows three behavior mechanical models, namely, the Maxwell model, the Voigt model, and the Kelvin model, all of which are composed of combinations of linear springs with spring constant μ and dashpots (pistons moving in a viscous fluid) with coefficient of viscosity η [10].

2.1.2.1 Maxwell Model

The "Maxwell" model shown in Figure 2.4 is a mechanical model in which a Hookean spring and a Newtonian dashpot are connected in series [11]. In that model, the stress on spring and dashpot, and the applied stress upon the model itself

are equal to each other. But, for the total strain it is not like that; it becomes the summation of the strain in both elements.

There is an exponentially stress reduction within time for Maxwell model. Moreover, it has a limitation that it does not indicate the creep truly. Although, big amount of strain rates of polymers falls down within time, the Maxwell model assumes that there will be a linear increase on strain rate when constant stress applied.

Some of the thermoplastic polymers, lots of metals and fresh concrete can be said as soft solids.

2.1.2.2 Kelvin-Voigt Model

The "Kelvin-Voigt" model shown in Figure 2.4 is a mechanical model in which a Hookean elastic spring and a Newtonian damper are connected in parallel. This model is used to consider the creep behavior of polymers. The spring and the damper move the same amount of distance. If the displacement is u and the velocity is ú. Then the forces that spring and damper produced, become μ u and η ú. Therefore the total force is shown;

$$F = \mu u + \eta \acute{u} \qquad \text{Eq. [2.1]}$$

As a linear first order differential equation, the Voigt model could be expressed;

$$\sigma(t) = \mu\varepsilon(t) + \eta \frac{d\varepsilon(t)}{dt} \sigma \qquad \text{Eq. [2.2]}$$

A solid undergoing reversible, viscoelastic strain was represented by this model. Upon the application of a constant stress, the material deforms with a decreasing rate, approaching the steady-state strain asymptotically. The material relaxes to its

un-deformed state gradually, when the stress is released. At constant stress (creep), as time continues to infinity, the model predicts strain to tend to σ/E. Like Maxwell Model, the Voigt Model also has limitations. While the model is very good with modeling creep in materials, it is much less accurate with regards to relaxation. Applications: rubber, organic polymers, wood (the load is not too high)

2.1.2.3 Standard Linear Model

The combination of a Hookean spring and the Maxwell model in parallel is called the standard linear model. Despite being modeled together both as a spring and as a damper within a given series, these two steady have a parallel relationship with a lone spring in a viscous material. The constitutive equation represented as:

$$\frac{d\varepsilon}{dt} = \frac{\frac{E_2}{\eta}\left(\frac{\eta}{E_2} + \sigma - E_1\varepsilon\right)}{E_1 + E_2} \qquad \text{Eq. [2.3]}$$

Rapid deformation on the modeled material into a random amount of strain is observed, upon the application of constant stress, namely the elastic portion of the strain. Deformation continues until it reaches a still strain state in an asymptotic way.

Given the specific conditions for loading, it is observed that despite being more accurate than other methods (Ex: Voigt, Maxwell), Standard linear model is actually inaccurate in mathematical terms, considering the results for the strain.

2.1.2.4 Generalized Maxwell Model

The basic constitutive elements of linear viscoelasticity are an elastic spring called Hooke-element and a viscous Newton-element. The elastic material constant μ gives the linear relation [12]. When the engineer considers it necessary to

incorporate this effect, the Wiechert model can have as many spring-dashpot Maxwell elements as needed to approximate the distribution satisfactorily [11]. Applications: alloys at temperatures lower than one quarter of their absolute melting temperature and metals.

2.1.3 Example Model of Viscoelasticity

Soft tissue modeling can be given as an example for this part.

2.1.3.1 Soft Tissue Modeling

Due to their flexibility, soft tissues may be distinguished from other body tissues like bones. This concerns the connective tissues, the muscles, the organs and the brain [13]. Body motion and deformation are entirely related with the mechanical properties of the soft tissues. In order to move skeleton, the muscles are responsible for force production. The tendons transmit this produced force to the bones to move our body's members. But due to our nature, bones have limited motions because of stable joints in our body.

In addition to that, the skin has an important function about protecting the organs from injuries. Soft tissues have different type of mechanical properties due to their structure rather than to the relative amount of their constituents [3].

Collagen can be considered as the main component of soft tissues. For example 75% of dry weights in human tendons, according to Elliot's reports, are represented by collagen. Elastin, ground substance, a type of hydrophilic gel, and reticulin take the burden of sharing the rest of the weight between themselves [14].

Skin is organized into two biaxial membranes: a relatively thin layer of stratified epithelium called the epidermis, and a thicker layer of disordered wavy coiled collagen and elastin fibers called the dermis (Figure 2.5) [15].

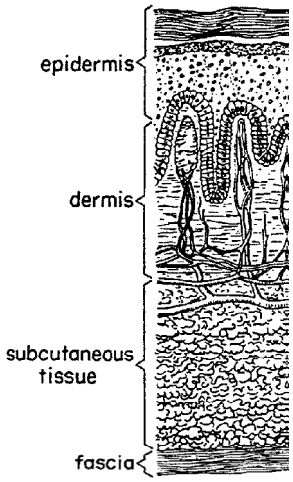

Figure 2.5 The skin layers [15]

2.1.3.2 Mechanical Properties of Soft Tissue

Non-linear Elasticity**:** It is the most important property for soft tissues. Kwan [4] described that: "Under uniaxial tension, parallel-fibered collagenous tissues exhibit a non-linear stress-strain relationship characterized by an initial low modulus region, an intermediate region of gradually increasing modulus, a region of maximum modulus which remains relatively constant, and a region is attributed to the removal of the undulations of collagen fibrils that normally exists in a relaxed tissue. As the fibrils start to resist the tensile load, the modulus of the tissue increases. When all the fibrils become taut and loaded, the tissue modulus a maximum value, and thereafter, the tensile stress increases linearly with increasing strain. With further loading, groups of fibrils begin to fail, causing the decrease in modulus until complete tissue rupture occurs." Figure 2.6 shows the typical tensile curve.

Viscoelasticity is the main criterion for investigation of soft tissue mechanical properties. A history-dependent component exists in the mechanical behavior of living tissues, when the equilibrium is not reached. In dynamic extension, the stress

values become higher than in equilibrium, for the same strain. So, the tensile curve appears steeper than that of an equilibrium (Figure 2.6).

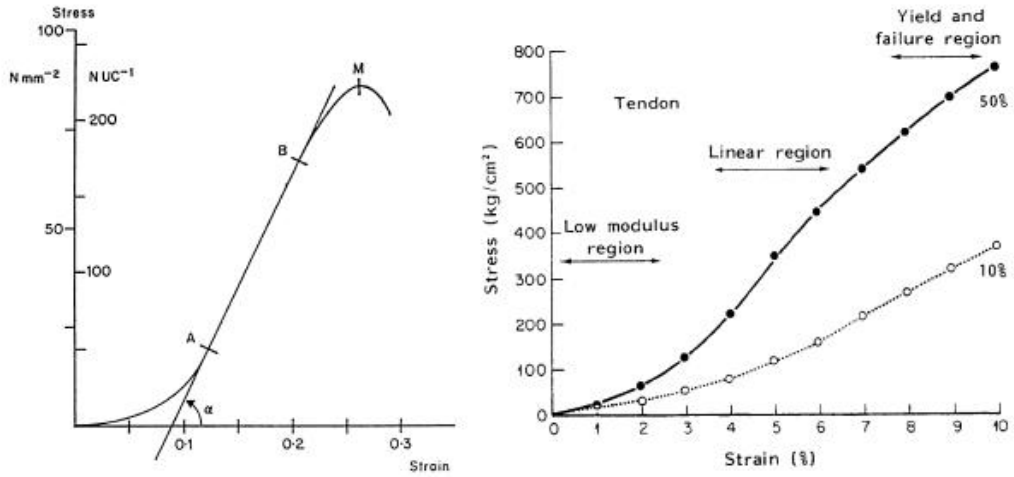

Figure 2.6 Load-Extension Curve (left) & Influence of the strain rate (right) [16]

2.1.4 Material Test Methods for Soft Tissue

Ex-vivo, In-vitro, In-vivo, Non-invasive, In-Situ test are test methods for soft tissue.

Ex-Vivo Tests Methods: In these tests, an organ is taken out of the organism as a first step, and their living conditions are tried to be duplicated by the help of various systems, enabling collection of more dependable and convenient data.

In-Vitro Tests Methods: In the in-vitro tests, an organ is taken out of its place in the organism, as in the ex-vivo tests. Tests are carried out on the dead tissues. In the in-vitro tests, duplication of the natural environment of the tissues is not a concern, and the tissue is studied is its raw form. In these tests, tissue may be studied as a whole or as divided to parts [17,18].

In-Vivo Tests Methods: In these tests, the organ is studied at its original place while it is still alive.

In-Situ Method**:** In these tests, organ is studied at its original place but the tissue is not alive.

2.1.5 Devices Used in Soft Tissue Test

It is possible to achieve tests on soft tissue by using different types of experiment devices. These devices can be selected according to the methodology and the requirements in the results. Compression, torsion, tension, suction and indentation tests are used for soft tissues [25]. The fallowing section, detailed information about indenter test can be found.

2.1.5.1 Indenter Tests

Methods which are frequently used in the investigation of the mechanical properties of soft biological tissues are the indenter tests for viscoelastic behavior [19]. Indenter tests possess many advantages and some of these merits are as follows:

1. Can be used in all tests methods. Thus comparative studies are feasible.
2. It is the most suitable method to be used in in-vivo tests.
3. Viscoelasticity, relaxation and creep behaviors as well as anisotropy in one plane [19], which are the important features of the soft biological tissues, can be examined by the tests where the indenter device is engaged. Relaxation and creep graphs can be plotted in experiments using indenters.

And also some disadvantages are as follows:

1. Indenter tips must be examined well especially in terms of their effects to results. Indenter and tip geometry is very important in penetration and also it must be simulated with correct dimensions in finite element analysis program.
2. Stabilization is another problem. Tested material must be fixed well to a stationary place to avoid noises.
3. Indenter test setup is created with combining different equipments such as force sensor and movement control unit. Equipments which are used in indenter test setup must be very sensitive and well controlled. Simultaneous working of different parts and their mutual loading is another issue to handle in an optimized manner.

These tests are made by the forward movement of the indenter tip towards the tissue and the simultaneous recording of the time, force and displacement data as given in the figure below.

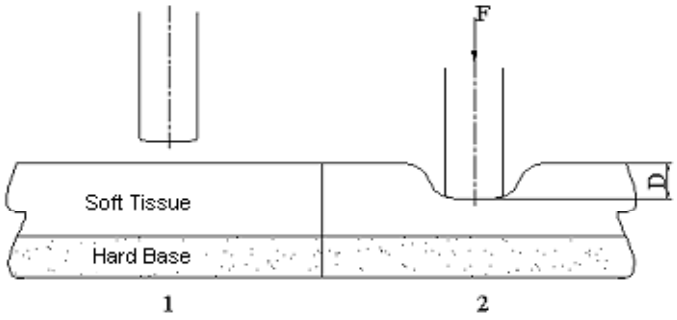

Figure 2.7 Indenter device loading representation
(1) Before loading the soft tissue by the indenter device. (2) After loading the soft tissue by the indenter device. Here, F is force and D is the distance traveled in the tissue. [19]

2.2 Definition of Elasticity and Hyperelasticity

Basically, elasticity can be described as a physical property of a material by which the material can return to its original shape after the stress that made it deform is removed.

A material can be called as a linear elastic material if it satisfies the following hypotheses [16].

- The elastic body is continuous and remains continuous under the action of external forces. According to this hypothesis the atomic structure of the body is disregarded and the body is idealized as a geometrical copy in Euclidean space whose points are set by the material particles of the body.
- The elastic body holds Hooke's law (linear relationship between stress and strain) which has the definition,

$$U = a_1 P_1 + a_2 P_2 + ... + a_n P_n \qquad \text{Eq. [2.4]}$$

Where,

U: Displacement (strain)

P_i: Force magnitude (stress)

a_i: Constants depend on the location of the point at which the strain is measured and points of application of the stress.

There exists a unique unstressed state of the elastic body to which the body returns whenever all the external forces are removed.

Up to a certain stress level, most solid materials exhibit such elastic behavior. This stress level is called yield strength of the material. If the stress surpasses this certain level, permanent deformation of the object will occur and the linear relationship that mentioned in second hypothesis between stress and strain no longer applies [20]. A stress-strain curve is one of the tools for visualizing this transition (Figure 2.8).

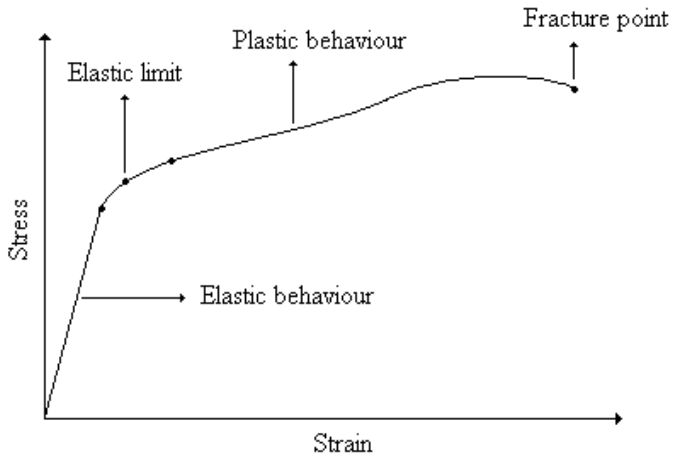

Figure 2.8 Stress-strain curve of a linear elastic material [20]

Furthermore, not only solids display elasticity. In response to a small, rapidly applied and removed strain, some fluids will behave as an elastic material. Above the critical stress, the "yield stress" these fluids may start to flow like a liquid, with some viscosity [21].

2.2.1 Hyperelastic Materials

Hyperelastic materials form a subclass of elastic materials. As mentioned previously, there is some behavior other than linear deformation to determine the stress state of an elastic material. However, hyperelasticity has a powerful assumption of the fact that all the factors other than deformation are not taken into account for determination of stress state. As a result, the stress state does not depend on the route followed during deformation process. In short, it can be inferred that hyperelastic materials are mathematically ideal form of elastic materials with the assumption given above.

To determine the behavior of hyperelastic materials, which shows quite much elastic response, finite element method which is used for many nonlinear problems of mechanics is chosen.

2.2.2 Properties of Hyperelastic Materials

A combined function of the shear (deviatoric) and volumetric components of strain tensor is used to get the strain energy density of hyperelastic material models. While doing this, the volumetric terms can be assigned as zero, hence calculating only shear terms, since it is assumed that rubber-like materials are incompressible, given the fact that this assignment of zero value for volumetric terms would not hold for all flexible materials.

Since it is important to get a hyperelastic model and material with multi-axial states, data derived from the tests are to be considered in terms of plane stress (uniaxial tension), plane strain (planar tension), volumetric compression and equi-biaxial (equi-biaxial tension), in order to get accurate results. The instruments and methods developed by NPL (National Physical Laboratory) are ideal for getting reliable input data, when applying test methods.

When considering the final bonded structure, it has to be carefully made sure that obtained mechanical property data by using bulk test specimens in their cure state, is similar to the adhesives properties.

Some materials, for example flexible adhesives, are prone to have specific temperature and strain rate properties of their own, which forces the tests applied to them to determine their hyperelastic model properties to be carried out at these specific and equal strain and temperature rates.

To this end, FEA software mostly applies its own routines for coefficient calculations, with the usage of least squares, to describe the hyperelastic behavior. Afterward, single element tests are applied to conclude the accuracy of the model.

2.2.3 Hyperelastic Material Modeling

Hyperelastic material models for phenomenological descriptions of observed behavior can be classified as:

- Mooney-Rivlin
- Ogden
- Polynomial
- Saint Venant-Kirchhoff
- Yeoh

Detailed information is given in finite element analysis section (Chapter 4) about hyperelastic material models.

2.3 Previous Studies

In this study, experimental setup and models of viscoelastic and hyperelastic materials which are used in ANSYS are adapted from Basdogan et. al. (2007). They used pig liver in their experiments. In other words, they worked with soft tissue and its material properties. The models for modeling viscoelastic (Prony Series) and hyperelastic (Mooney Rivlin) for finite element are taken from Basdogan et. al. (2007). Due to this point, soft tissue modeling is the guidance for our modeling viscoelastic and hyperelastic material in finite element program.

Their inverse finite element method and optimization process are different than our study. In our research, an algorithm is created to simulate viscoelastic model in ANSYS. Optimization tool and its algorithm are also used for optimizing material model coefficients in ANSYS.

Basdogan et. al. (2007) explains that soft tissues' material characteristics display a rate and time dependent behavior, along with complex nonlinear, anisotropic and

non-homogenous properties. In their survey, they refer to Fung's (1993) theory of nonlinear stress-strain relationship being common for soft tissues, with the acknowledgement that the degrees being different for different tissues. Body motion and deformation are entirely related with the mechanical properties of the soft tissues. According to Fung (1993), soft tissues have different type of mechanical properties such as viscoelasticity and due to their structure rather than to the relative amount of their constituents [3].

Non-linear elasticity is the most important property for soft tissue and also for viscoelasticity. Kwan (1985) describes it as: "Under uniaxial tension, parallel-fibered collagenous tissues exhibit a non-linear stress-strain relationship characterized by an initial low modulus region. And an intermediate region of gradually increasing modulus, a region of maximum modulus which remains relatively constant, and a region are attributed to the removal of the undulations of collagen fibrils that normally exists in a relaxed tissue. As the fibrils start to resist the tensile load, the modulus of the tissue increases. When all the fibrils become taut and loaded, the tissue modulus a maximum value, and thereafter, the tensile stress increases linearly with increasing strain. With further loading, groups of fibrils begin to fail, causing the decrease in modulus until complete tissue rupture occurs [4].

Viscoelasticity is the main criteria for investigation of soft tissue mechanical properties. A history-dependent component exists in the mechanical behavior of living tissues, when the equilibrium is not reached. In dynamic extension, the stress values become higher than in equilibrium for the same strain. So, the tensile curve appears steeper than on at equilibrium.

The other main criterion for our study is hyperelasticity. Additionally to Basdogan et. al. (2007), Svecova [5] Mooney – Rivlin Theory is used for hyperelastic problem solution to set incoming material constants of tread rubber compounds [5]. With this study, they have defined characteristics of hyperelastic materials with

experimental tests and verified them with the use of finite element method simulation. In detail, the hyperelastic coefficients of the models have been calibrated by ABAQUS (commercial software, capable of wide material modeling, from experimental stress-strain data).

By implementing the mentioned process, Svecova has tried to optimize the material constants A and B of hyperelastic materials in the equation below:

$$\frac{\sigma_1}{2(1-\frac{1}{\lambda_1^3})} = A\lambda_1 + B \qquad \text{Eq. [2.5]}$$

Where,

A and B: The hyperelastic material constants searched for. They are also called Mooney-Rivlin constants.

λ_1: The main strain ratio

σ_1**:** The developed stress in test sample.

According to the study Svecova the Mooney-Rivlin coefficients from linear regression in MS EXCEL and ABAQUS are as the following:

Table 2.1 According to the study of The Mooney-Rivlin coefficients from linear regression from two different software tools

Table 2.1 The Mooney Rivlin Coefficients

Tool	**A (MPa)**	**B (MPa)**
MS Excel	0.1791	0.587
Abaqus	0.2608	0.3668

As explained above, an experimental setup must be prepared to collect required data by suitable test method. Various test methods are used in literature such as ex-vivo,

in-vitro, in-vivo, non-invasive and indenter test and they are expressed detailed in this chapter's below sections. Indenter test method is used both in our study and Basdogan et. al. (2007). And the similar haptic device based (robotic indenter) experimental setup are prepared. In our study, a new controller interface and graphical user interface are coded to control experiment processes.

Basdogan et. al. (2007) refers to Rosen et. al.'s (1999) design of a laparoscopic grasper being equipped with strain gages, to conduct experiments on porcine liver. Following this, it is referred to Ottensmeyer's (2001) design of a robotic indenter for measurement of mechanical properties. This probe could perform small indentions in the range of +/- 500 micrometers. His in-vivo experiments describe the elastic modulus of pig liver as 10-15 kPa. Following his footsteps, Tay et. al. (2002) achieved an indention depth of 8 mm via the usage of a commercial robotic arm. These experimental results were analyzed by Kim (2003) as 3-4 kPa of elastic modulus for pig liver. A robotic device, engineered by Desai and Hu (2004), performs further enhanced compression tests. These tests measure the force and displacement response of pig liver. Via their in vitro experiments they developed more efficient methods to estimate material properties from experimental data.

After data collection process, inverse solution must be formulated for all simulations. By this way, unknown material properties of measured response can be formulated. Hence a finite element model is to be constructed [1]. This model is to be optimized so it can match the experimental data. Our study has same process with different methods. For example, ANSYS Goal Driven Optimization method is used for optimization in our studies when compared with other studies.

Our own estimations and initial experimental setup values were referenced from Basdogan et. al. (2007) and their findings.

CHAPTER 3

EXPERIMENTAL SETUP

3.1 Problem Characteristics

Material model selection may generally be difficult due to material behavior such as viscoelasticity consequently one may want to relay an experimental tests materials in order to select the correct material models and their coefficients to be justified in simulation. There are lots of material test methods available in literature, which each yield different type of results gathered into related graphs and different test performance analyses.

In this study, our performance acquisition is an optimization process that is directly related with stress relaxation graph of selected materials. Stress relaxation is one of the main properties of viscoelasticity so we try to optimize the selected material model coefficients according to stress relaxation data. And another fact is that in our finite element analysis simulation, stress relaxation test is simulated for a material used in the optimization process.

In order to specify the mechanical characteristics of the material being tested, indenter test method is selected as experimental method. Since it is a highly versatile setup and it is possible to identify viscoelasticity, creep and relaxation behaviors on a single plane and to plot relaxation (counter force reaction) graphs of acquired data. The acquisition of the data makes possible the identification of the material coefficients of the tested material, using of proper procedures. Detailed

information about indenter tests and its advantages – disadvantages can be found at literature survey section.

3.2 Requirements for the Experimental Setup

In the indenter test setup, high sensitive and accurate equipment is needed. In order to obtain proper material coefficients due to experimental data, the relaxation graph of the test has to be very accurate for optimization. The control device and force sensor have to process and control in real time with the computer. The computer then plots the graphs of changes in force values, even the slightest ones by using coded algorithm and its user interface.

In order to plot relaxation (counter force reaction) graph of the experimented material and comment on the results, a specific experiment setup has been prepared in our experiments, via below explained equipment. This procedure and the equipment used in the experiment will be explained in detail in this chapter.

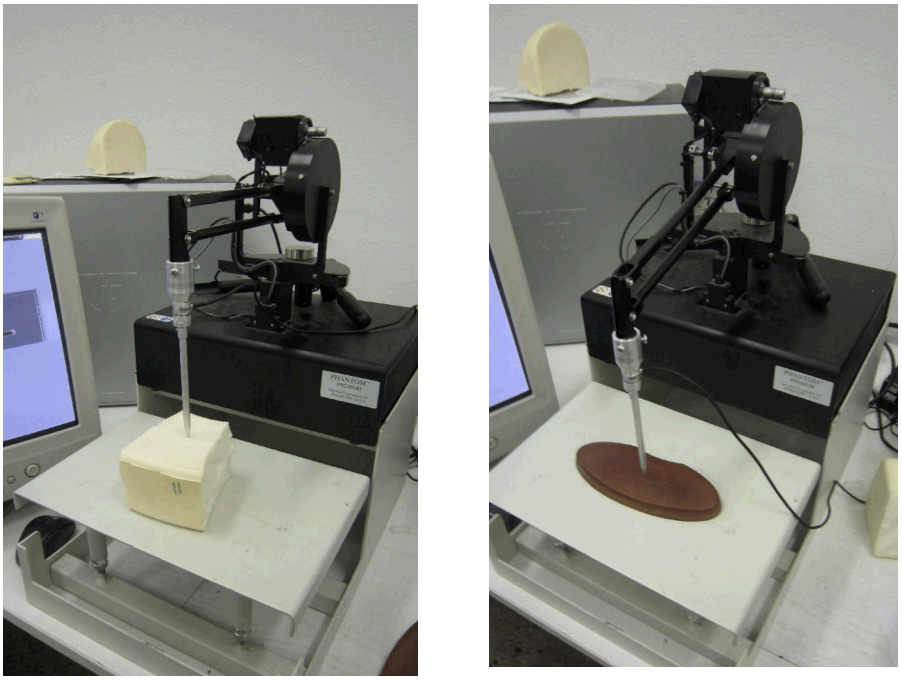

Figure 3.1 Experimental Setup

3.3 Experimental Setup

The main equipment of the mechanism is a haptic device that we used in order to control the penetration of the probe into the material in a very accurate and sensitive way. With the encoded interface and help of prepared GUI (Graphical User Interface), the haptic device can move to any desired direction, which enables the penetration depth of the indenter's path, the waiting time of the probe in the material, and the speed and input time of the indenter into the material.

With the help of Force Sensor, the force values are acquired real time, and their graphs are plotted synchronously in the GUI during the experiment. The Data Acquisition Card in the setup gathers and sends the data at the desired sample rate from the force sensor to the computer, and enables the GUI to process and plot. Our GUI enables us to adjust the sample rate to be acquired. The Data Acquisition Card allows us to get 1000 data per second (1000 Hz). Sample rate can be adjustable from encoded interface. Hence, the sample rate has been determined as the maximum value in our experiments.

Furthermore, some materials have been manufactured, in order to connect these main components. Detailed information of the materials in our test setup is given in below.

3.3.1 Haptic Device

Haptic interaction with the world is manipulation using our sense of touch. The term "haptics" arises from the Greek root haptikos, meaning "able to grasp or perceive."

Haptic devices are used to provide three dimensional data transfer between haptic users and computers in virtual reality applications. They enable humans to take

force and tactile feedback from any virtual or remote objects. Haptic devices also facilitate the use of data collected from a real object in the virtual environment [22].

Different types of haptic devices can be used in order to give interaction with the whole body or some organs. Nowadays haptic systems are used in robotics, games, simulators, medicine, art, etc.

With the help of the libraries and algorithms, supplied by companies, haptic devices can be used in many other areas and applications. Controllable robot arm can be given as an example to this subject

In our studies, PHANTOM® Premium 1.5/6-DOF HF, of the brand Sensable, has been used as our haptic device, with its picture shown below in the data sheet appendix. Its workspace is 381x267x191and its nominal position resolution is 3784 in translational.

Figure 3.2 Phantom Premium Haptic Device

We removed last three joint from the haptic device, in order to mount our own adapter, which holds the force sensor and the probes, and in order to secure a

desired movement. With this modification, the haptic device was able to move given path in its working area and penetrate to the surface of the material, as shown in Figure 3.1. Since we removed last tree joints, in order to position the tip point of the haptic device, we developed our own controller interface and GUI, which is to control the movement of haptic device.

We were able to move the indenter connected to the haptic device via the force the motors upon the haptic device. During the experiment the indenter moves along its path with negligible errors (0.01mm deviation). Proportional Integral Derivative Controller (PID Controller) helps the indenter with its movement by controlling the forces which act on haptic device's motors. This PID Controller is embedded to the control interface beforehand. The indenter is in a fixed position during the experiment or calibration, and it moves to desired positions with very small errors. With the help of the PID, when we run our GUI, we can observe the errors in real time.

Before the experiment, the indenter has to be placed perpendicular to the material surface, its position has to be calibrated and it has to stand still for a while before starting. The reason for standing still for a while is PID's accurate calculation and placement of indenter upon the calibration point, hence converging the error values near to zero, and enabling us to conduct our experiment in a stable way. With the help of GUI, our experiments become automated, which is explained in GUI chapter.

3.3.2 Force Sensor and Data Acquisition Card

To measure the force values in the experiment, ATI Force sensor NANO 17 (SI-50-0.5) is used. In order to transfer the values measured in by the force sensor, a data acquisition card of the brand NATIONAL INSTRUMENTS, PCI 6052e model is also used.

The rated sensing rates ranges of ATI NANO 17 Force Sensor are ±50 N for both Fx and Fy, and with resolution of 1/160 N. For Fz the same properties have the values ±70 N and 1/320 N resolution. Corresponding torque values Tx, Ty and Tz have the range ±500 Nmm.

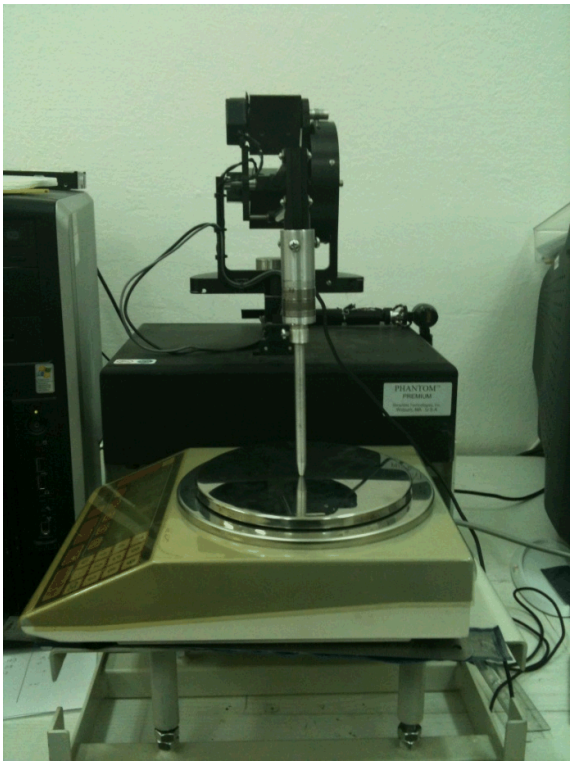

Figure 3.3 Force Sensor Calibration

Force sensor has been calibrated after the experimental setup was prepared, in order to get proper readings. A file, calibration.dat, has been added to the interface, taken from ATI. This file is different for each force sensor so exact calibration data must be selected. To check correction of force sensor, the precision balance scale in the picture show above has been used for comparing force data. After these steps, it has been concluded that calibration.dat is proper and the measured values have been verified.

A process, called bias, has to be applied before the experiment, in order to nullify the indenter value on the force sensor. This has to be done after the calibration of the position of indenter. The button “Bias” is active in our GUI only after the indenter calibration, and it nullifies the indenter weight on the force sensor. This enables us to observe the force reaction (counter force) of only the tested material during the experiment.

Since the force sensor used in the experiment is very accurate and sensitive, there is some noise in the resulting data. Low Pass Filter has been used, in order to reduce the noise in our data. This filter has been implemented into our interface as well. In our GUI we have the option of filtering directly, after the experiment has been finished.

The operating system of the computer where we had our experiment is Windows XP, and the computer itself is HP Workstation xw8200.

3.3.3 Manufactured Materials

As mentioned earlier, some required materials have been fabricated in order to complete our experiment setup. The probe has been manufactured from aluminum, as well as the adapter, which connects the force sensor and the probe. Below are their pictures.

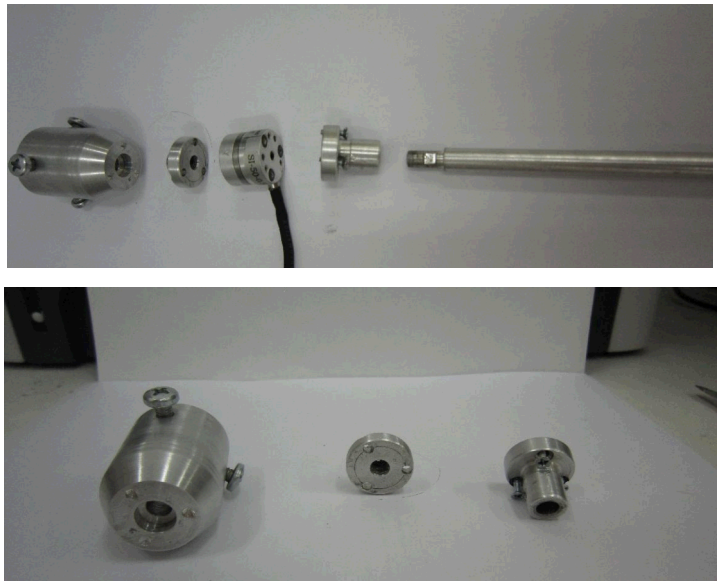

Figure 3.4 Force Sensor Adaptor and Probe

A chassis has been created, in order to place the haptic device upon it. With the help of its adjustable base structure, we could place the experimented material into the best fitting slots according to the haptic device. Also, with the help of this chassis, the experimental system became stable, hence prohibiting vibrations, which can cause noise in the force data.

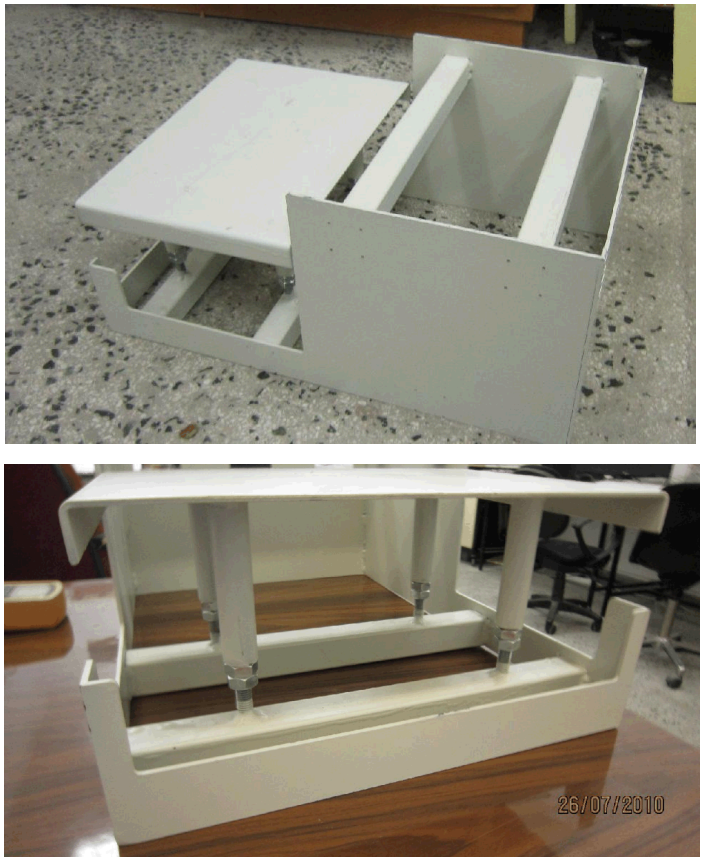

Figure 3.5 Manufactured Chassis

3.3.4 Controller Interface and GUI

As mentioned previously, an interface controller has been coded earlier, in order to automate the mechanical system of the experiment, record the resulting data and apply the necessary processes. This interface was coded in C++, and a GUI has been created for this specific interface. This GUI, with the help of algorithms, enabled the processing of all data acquired from the experiments, and control of the results, hence automating the experiment, prohibiting possible errors during the experiment or its procedures. It also enables us to obtain raw and filtered graphs of the resulting experimental data, with respect to time. With the analysis of both previously introduced materials' (Gel, foam viscoelastic material, soft tissue) force reaction graphs and tested materials' force reaction graph, it can also calculate

possible model coefficients for optimization by determining to which structure our material is closer to.

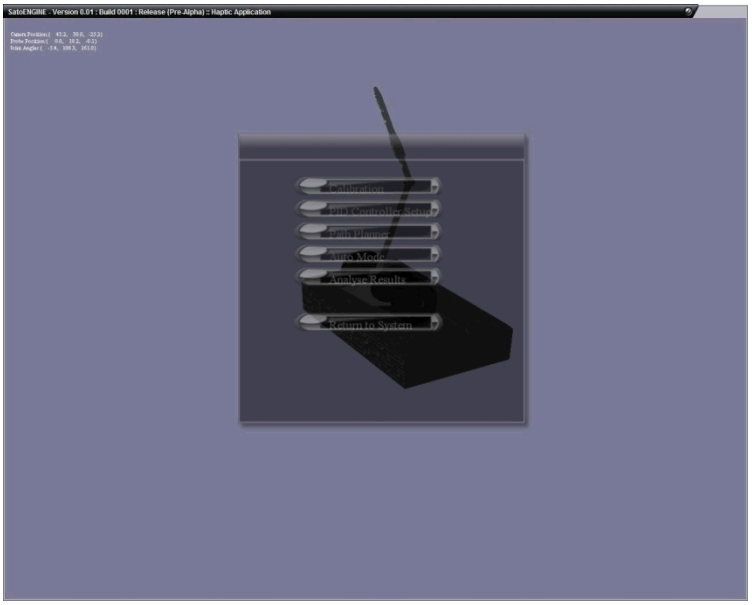

Figure 3.6 Controller Interface

Figure 3.6 is the main menu of our GUI. The simulation of the haptic device is both here and also in experiment menus. This simulation displays the movement of the haptic device in computer environment. The movement of the indenter can be observed from the computer during the experiment. Other menus in order are Calibration, PID Controller, Path Planner, Auto Mode and Analyze Result. Below are the explanations for each of these menus.

Figure 3.7 PID Menu

As mentioned earlier, since we apply a position control via force in haptic device control, PID control has been coded, in order to check force feedbacks and protect the system from vibrations. Discrete PID has been used as PID controller. Values of PID can be changed via PID controller in the menu, in real time. With these values, we can observe the errors on the path of indenter and its current position in real time, hence making very accurate and sensitive turns. PID values differ between different materials, and new tuning is applied for new material. Below is a detailed explanation about discrete PID.

PID:

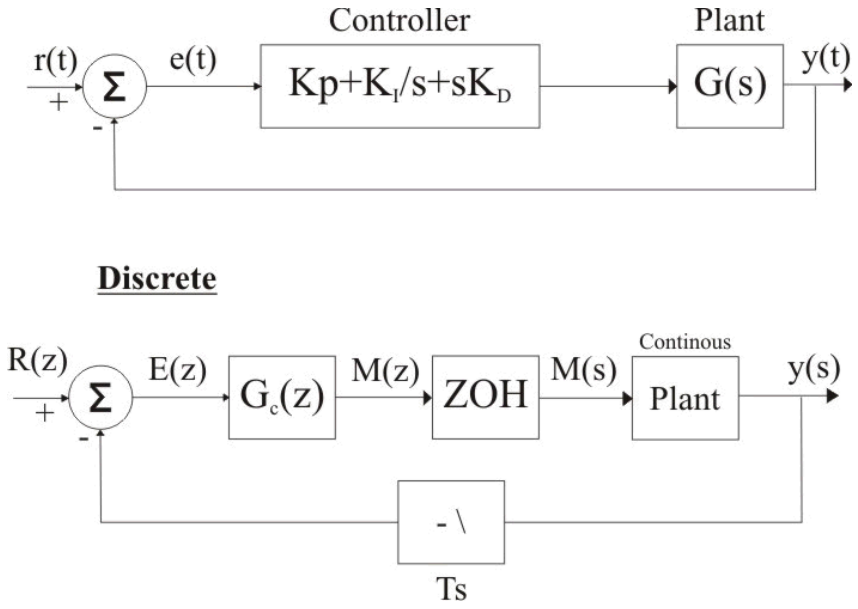

Figure 3.8 Block Diagram of PID

Mathematically:

$$m(k) = m(k-1) + b_0 e(k) + b_1 e(k-1) + b_2 e(k-2) \qquad \text{Eq. [3.1]}$$

$$b_0 = Kp + \frac{Kd}{Ts} + KiTs \qquad \text{Eq. [3.2]}$$

$$b_1 = -Kp - \frac{2Kd}{Ts} \qquad \text{Eq. [3.3]}$$

$$b_2 = \frac{Kd}{Ts} \qquad \text{Eq. [3.4]}$$

In PID system increasing P value produces faster responses and larger overshoots to system. By this way, system will resist to possible disturbances. But steady state error remains constant. Increasing I value makes steady state error lower but this time response time will get slower. Value D has no visible effect on slow

disturbance. In additionally, it gives damping effect to the dynamic response on system.

Figure 3.9 Path Menu

Movement of the indenter can be observed and controlled under Path Planner menu, or via an outsourced script. The rate of penetration upon the surface of the material, the time of waiting inside the material, or creation of a new path and new waiting durations can all be adjusted for the experiment. This enables haptic device and the attached indenter to be used in different experiments.

Once the path is established and automated experiment option is chosen, indenter calibrates and its force sensors are biased. Indenter starts moving according to the established path. During the movement, the force sensor measures the reaction forces from the material. In the mean time, the data acquisition card records these measured values.

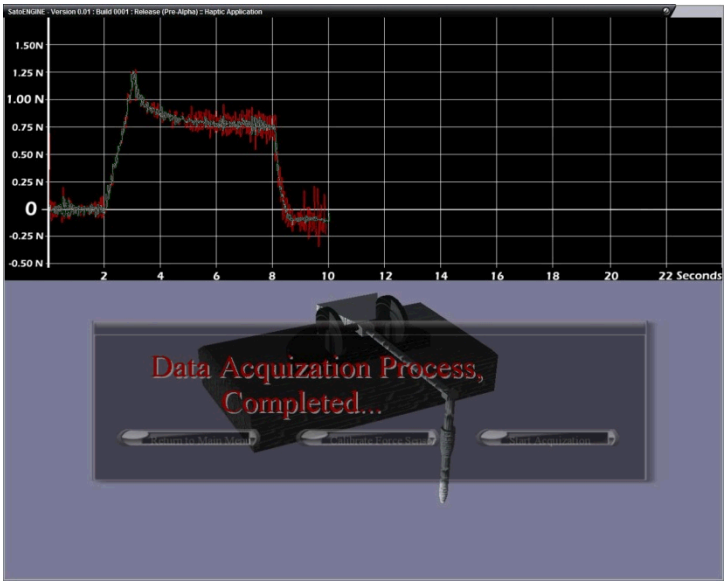

Figure 3.10 Data Acquisition Menu

Once the path has been established for the experiment and the indenter calibration and biasing is finished, the experiment starts, and the data from the force sensors displayed in GUI in real time. As shown above, these data represent the force relaxation graph of the material. In above graph, red represents raw data. With the help of embedded Low Pass Filter, raw data can be filtered after its acquisition. In the same graph, green represents filtered red data. All these data are recorded into a script in notepad, with respect to time.

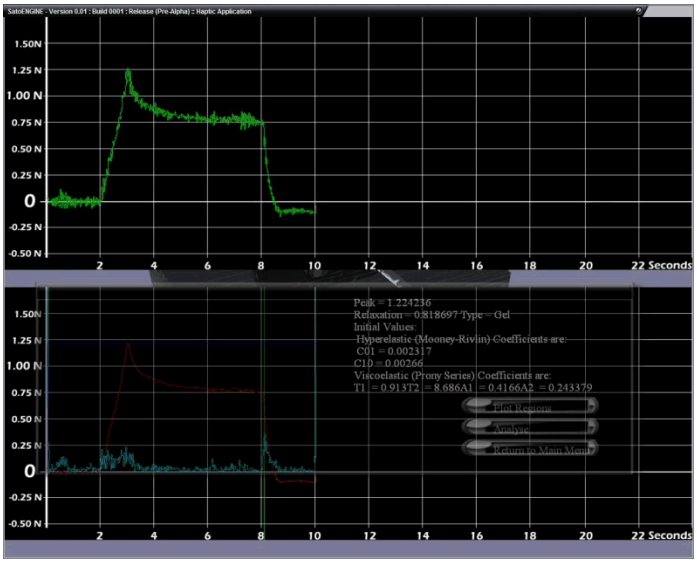

Figure 3.11 Analyses Menu

Our GUI analyzes the stress relaxation graph of tested material according to their resulting data, after the experiment is finished and filtered data are acquired. If the experimented structure is similar to a previously introduced viscoelastic structure, the GUI presents initial material coefficients, to be used in optimization.

First stress relaxation test must be done to new viscoelastic material to get initial material coefficients for optimization. When test is completed GUI automatically filter the test data. After that, user can press “Analyze” button to get initial material coefficients.

Stress relaxation graph of tested material must be similar to viscoelastic material’s relaxation graph to get initial material coefficients. In our experiment setup, viscoelastic materials (Gel, Foam, and Soft Tissue-Arm) have been introduced to the interface algorithm, hence this option can only be used in viscoelastic materials.

With the help of analysis and their resulting values, material coefficient optimization starts with more accurate values, which are closer to ideal.

Optimization is applied with smaller error margins and the duration of optimization is reduced.

CHAPTER 4

FINITE ELEMENT ANALYSIS

4.1 Introduction

Main goal of this part is to simulate finite element model with the viscoelastic and hyperelastic properties of the tested material by using inverse finite element method and preparation process for optimization. Tested material behaves in a non-linear way and therefore the proper material model cannot be found within the material library of ANSYS. So the main problem in our simulations is the selection of material model. A special model was simulated for solving the tested material's viscoelastic and hyperelastic properties in the same analysis. This model contains ANSYS hyperelastic model (Mooney-Rivlin) and an external algorithm (Prony Series) for simulating a viscoelastic model. Algorithm was coded by using APDL (ANSYS Programming Design Language) and explained in previous chapters. All finite element simulations and optimization processes were done with ANSYS 11.0 and its sub-programs called Workbench and DesignXplorer.

Simulation of experiments in ANSYS is also important. They are time dependent and because of this, simulations have to be done by using flexible dynamic analysis to check time steps correctly, in order to create accurate relaxation graphs. Relaxation test data (counter force – time) of tested material is the main optimization criteria in these simulations. To test material's relaxation graph, goal driven optimization method is used. Consequently, relaxation graph is directly

related to material's hyperelastic and viscoelastic coefficient, which means, that optimizing the material's coefficients is also important.

Necessary steps for making a non-linear and flexible dynamic analysis are shown below;

- Define the geometry
- Assign material properties
- Define contact options
- Define mesh controls
- Include load and supports
- Request results
- Set nonlinear solution options
- Solve model
- Review Results

Main properties and difficulties of the modeling tested materials are;

- Material Nonlinearity
- Large Deformation

4.2 Material Nonlinearity and Nonlinear Analysis

There are three main non-linearity sources, named as geometric, material non-linearity and contact. Corresponding definitions are given below;

Geometric: If a structure experiences large deformations, geometric configuration change can cause nonlinear behavior.

Material Nonlinearity: A nonlinear stress-strain relationship shown in Figure 4.1, is another source.

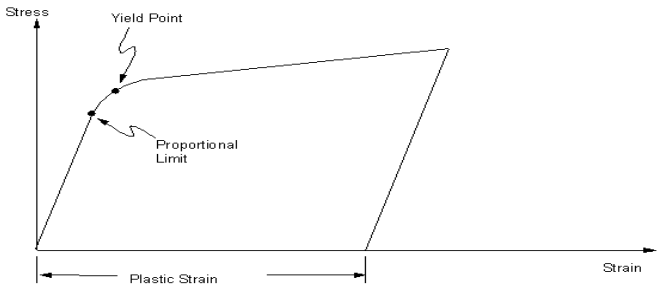

Figure 4.1 Stress strain relationship causing Material Nonlinearity [23]

Contact: Adding a contact effect to non-linear models makes the system unstable, since, in case of contact between two bodies there is a sudden change in the stiffness values.

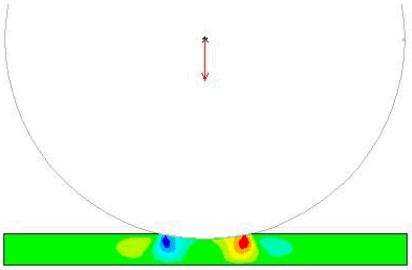

Figure 4.2 Contact Nonlinearity [23]

To understand the concept of non-linear analysis, the basic structure of static analysis has to be examined. In non-linear static analysis, the stiffness [K] depends on displacement {x}:

$$[K(x)]\{x\} = \{F\} \qquad \text{Eq. [4.1]}$$

The resulting force versus the displacement curve is non-linear. Main purpose of the non-linear analysis is being an iterative solution where the relationship between

load (F) and response (x) is not known before. Time-dependent effects are not considered.

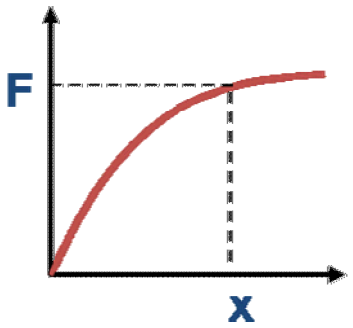

Figure 4.3 Nonlinearity between load and response [23]

ANSYS Workbench simulation performs certain types of non-linear static structural models. In our model, a large deflection and a non-linear contact behavior have been added to the structure of the analysis. With these properties, non-linear analysis can be done more efficiently. Viscoelastic properties of tested material are also linked to model.

Non-linear analysis requires several iterations. The actual relationship between the applied load and the deformation is not known previously. To solve the relationship between them, the Newton-Raphson method, which can be thought as a series of linear approximations with corrections, is performed.

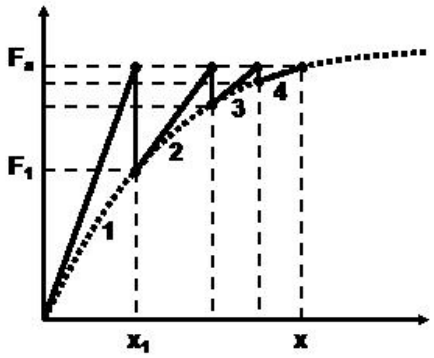

Figure 4.4 Newton-Raphson Method [23]

In Figure 4.4, F values are applied and response forces and x values are displacements. In this method, the forces are applied to the structure in order. Based on the newly deformed shape, the internal F_1 are calculated. In case that the system is not in equilibrium at this point, a new stiffness matrix [K] is calculated based on the current conditions. This process is repeated until the solution is converged for all a, with a=1, 2, 3, …, i. The applied load F_a has to be split into smaller increments for convergence. Hence, for a ramped load, small time stamps are preferred. The time stamps will also have an influence on the linear analysis. They should be small enough to allow the Newton-Raphson method to obtain force equilibrium. The user should specify the initial, minimum and maximum time steps, based on non-linear considerations.

ANSYS Workbench simulations use only one set of time steps when resolving the dynamic response. These time steps can be small enough to resolve non-linear effects. Determination of these time steps, based on non-linear considerations is not an easy task, as the choice of dynamic time steps size. Hence, the user may rely on an automatic time-stepping algorithm to ensure convergence and accuracy. The automatic time stepping algorithm takes the following non-linear effects into account:

- If force equilibrium is not satisfied, bisection occurs.

- If an element has excessive distortion, bisection occurs.

Bisections are part of the automatic time stepping algorithm. When the solver goes back to the previously converged solution at the time t_i, bisections are created with smaller time increments Δt_i. Bisections provide automated means to solve nonlinear problems more accurately or to overcome convergence difficulties. Bisections result in wasted solver time since the solution returns to the previously converged solution and tries again with a smaller time step. Hence, choosing the right initial and maximum time steps can minimize trial number and increase the speed of simulations.

In default settings for non-linearity, large deformation effects and automatic time stepping is active. In our model, non-linear effects dominate and the time stamp sizes are calculated by concerning non-linear considerations.

4.3 Large Deformation

Most of the viscoelastic materials can be modeled as non-linear elastics by using pseudo-elasticity. Any material having a strain ratio greater than 3% to 5% means Large Deformation. When the deformation is too small, volume change in material is negligible and for material modeling, hence, linear strain tensor and the Cauchy stress tensor can be used. In large deformations greater than %5 strain, constitutive relations have to be used in this model.

In ANSYS, both static structural analysis and flexible dynamic analysis can be performed. It also determines whether the large deformation effects such as large deflection, large rotation and large strain should be taken into account. In the program, we set “Large Deflection” to on if we expect large deflections or large strains. If we use hyperelastic material models, we must set “Large Deflection On”, because in hyperelastic materials there is large deformation under loading.

In a large deformation analysis, ANSYS automatically updates the nodal coordinates of the model's solution, and then proceeds to the final configuration. In previous chapters, the effects of large deformation and solution processes were explained in detail.

4.4 Structure of the Finite Element Model in ANSYS

4.4.1 Model

Finite element model tree was created using ANSYS. This model tree defines the geometry for the particular sub-groups of the main structure. With this model, other model properties such as mesh, connections etc. were given in an essential order. The sub-groups provide additional information about the model object such as loads and supports.

Table 4.1 Units of experimental conditions

Units	
Unit System	mm, kg, N, ^{O}C, s,
Angle	Degrees
Rotational Velocity	rad/s
Temperature	22 ^{O}C *

* Which is neglected but required for simulation

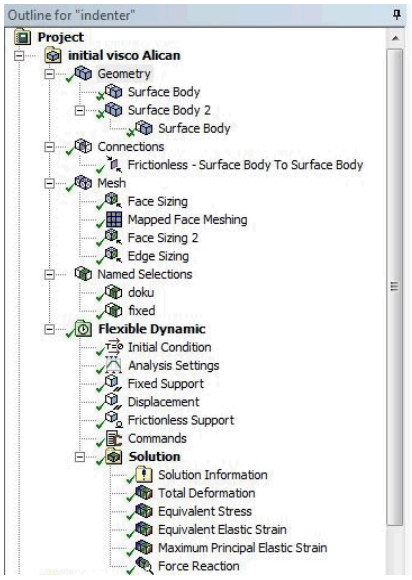

Figure 4.5 Model Tree of ANSYS

4.4.2 Geometry and Material Selection

Geometry of the tested material and indenter were created in Designmodeler in ANSYS. Designmodeler is a geometry editor and a parametric feature-based solid modeler. Users can draw 2D sketches and easily convert them into 3D models.

The geometry of indenter was drawn and named as “Surface Body 1”. Tested material was simplified to 2D rectangle and named as “Surface Body 2”. Behavior of these sketches is axisymmetric, which means that 3D model can be generated by revolving a 2D section about 360^{o} the y-axis. The axis of symmetry must coincide with the global y-axis [23].

Indenter’s dimensions are 2 x 20 mm with rectangular shape. Material of indenter was selected as aluminum (Also, our experiment indenter is made of aluminum). Material properties, automatically loaded from material library of ANSYS, are called Engineering Data. In Engineering Data, users can change selected material

properties like Young's Modulus and Poisson's Ratio etc. or create a new material with custom properties.

Tested material was represented by a 2D, 25 x 20 mm rectangle. It was generated to create finite element algorithm and whole FEA solutions and optimizations were based on this element.

New material was added to Engineering Data with a name "doku_int" and has been assigned to tested material. Main goal is to determine the material properties and the structure of tested material. For this reason, inverse finite element method structure was built by using hyperelastic and viscoelastic models. By doing this, we determine the coefficients of viscoelastic and hyperelastic of the tested material. ANSYS library includes hyperelastic models but viscoelastic models are not included in the library.

4.4.3 Hyperelastic Material Finite Model for Tested Material

As previously mentioned, hyperelasticity refers to the materials which can experience large elastic, strains which is recoverable [23]. For example rubbers and all other polymeric materials are hyperelastic. An example to polymeric materials is elastomers, with their polymer solid structure and chain like molecules. It gives flexibility and they usually behave elastically isotropic. Common properties are;

In elastic response, if the stresses are lower than the material's yield strength, the material can fully recover its original shape upon unloading.

- From a standpoint of metals, this behavior is due to the stretching but not breaking of chemical bonds between atoms. Because elasticity is due to this stretching of atomic bonds, it is fully recoverable. Moreover, these elastic strains tend to be small.

- Elastic behavior of metals is mostly described by the stress-strain relationship of Hooke's Law:

$$\sigma = E\varepsilon \qquad \text{Eq. [4.2]}$$

- They can undergo large elastic deformations. There is little volume change under applied stress since the deformation is related to straightening of chains. Hence, they are nearly incompressible.
- Their stress-strain relationship can be highly nonlinear.
- Usually, in tension, the material softens then gets stiffer again. On the other hand, in compression, the response becomes quite stiffer.

There are key assumptions related to the hyperelastic constitutive models in ANSYS. Material response is isotropic, isothermal and elastic. Thermal expansion is isotropic but not related with our simulations. Deformations are fully recoverable. As mentioned before, material is fully or nearly incompressible and idealized as a true rubbery behavior, which is more complex.

The constitutive hyperelastic models are defined through a strain energy density function. Hyperelasticity is not defined as a rate formulation. Instead, total-stress versus total strain relationship is defined through strain energy potential (W);

$$\dot{\sigma} = D : \dot{\varepsilon} \qquad \text{Eq. [4.3]}$$

The stretch ratio is defined as,

$$\lambda = \frac{L}{L_0} = \frac{L_0 + \Delta u}{L_0} = 1 + \varepsilon_E \qquad \text{Eq. [4.4]}$$

Above is an example of stretch ratio which is defined for uniaxial tension of a rubber specimen, where ε_E is engineering strain. There are three principal stretch ratios λ_1, λ_2 and λ_3 which will provide a measure to the deformation. These will also be used in defining the strain energy potential. The principal stretch ratios λ_1 and λ_2 characterize in-plane deformation On the other hand, λ_3 defines the thickness variation (t/t_o). Additionally, if the material is assumed to be fully incompressible, then λ_3 will equal to λ^{-2}.

The three strain invariants are commonly used to define the strain energy density function.

$$I_1 = \lambda_1^2 + \lambda_2^2 + \lambda_3^2$$
$$I_2 = \lambda_1^2\lambda_2^2 + \lambda_2^2\lambda_3^2 + \lambda_3^2\lambda_1^2 \qquad \text{Eq. [4.5]}$$
$$I_3 = \lambda_1^2\lambda_2^2\lambda_3^2$$

If a material is fully incompressible then $I_3=1$.

Assuming that the material is isotropic, some forms of the strain energy potential are expressed as a function of scalar invariants. In other words, strain invariants are measures of strain which are independent of the coordinate system used to measure the strains. So, we can use isotropic material behavior in our assumptions.

The volume ratio J can be defined as;

$$J = \lambda_1\lambda_2\lambda_3 = \frac{V}{V_0} \qquad \text{Eq. [4.6]}$$

As shown above, J can be thought as the ratio of deformed (V) to undeformed (V_0) volume of the material.

In the case of thermal expansion, the thermal volumetric deformation is

$$J_{th} = (1+\varepsilon_{th})^3$$
$$J_{el} = J = \frac{J_{total}}{J_{th}}$$
$$W = W(I_1, I_2, I_3)$$
$$W = W(\lambda_1, \lambda_2, \lambda_3)$$

Eq. [4.7]

The elastic volumetric deformation is related to the total and thermal volumetric deformation by the following equation:

$$J_{el} = J = \frac{J_{total}}{J_{th}} \qquad \text{Eq. [4.8]}$$

The strain energy potential (or strain energy function) is usually denoted as W and it can either be a direct function of the principal stretch ratios or a function of the strain invariants.

$$W = W(I_1, I_2, I_3) \qquad \text{Eq. [4.9]}$$

or

$$W = W(\lambda_1, \lambda_2, \lambda_3) \qquad \text{Eq. [4.10]}$$

The particular forms of the strain energy potential determine whether stretch ratios or strain invariants are used. However, instead of using principal stretch ratios or strain invariants directly, modified forms can be also used. Because of material

incompressibility, we split the deviatoric and volumetric terms of the strain energy function. As a result, the volumetric term is a function of volume ratio J only.

$$W = W_d(\bar{I}_1, \bar{I}_2) + W_b(J)$$
$$W = W_d(\bar{\lambda}_1, \bar{\lambda}_2, \bar{\lambda}_3) + W_b(J) \qquad \text{Eq. [4.11]}$$

where the deviatoric principal stretches and deviatoric invariants are defined as (for p=1, 2, and 3);

$$\bar{\lambda}_p = J^{-\frac{1}{3}}\lambda_p$$
$$\bar{I}_p = J^{-\frac{2}{3}}I_p \qquad \text{Eq. [4.12]}$$

Hence, the use of $\bar{\lambda}_p$ and $\bar{I}_p$ allows separation of W into deviatoric and volumetric terms. Note that $I_3 = J^2$, so I_3 is not used in the definition of W.

Through the strain energy function, the stresses and strains can be calculated. So, conjugate measures of stress and strain should are used. For example based on W, second Piola-Kirchoff stresses are determined as;

$$S_{ij} = \frac{dW}{dE_{ij}} \qquad \text{Eq. [4.13]}$$

ANSYS results show true stresses and true strains. Curve fittings used in simulations requires engineering stresses and engineering strains.

4.4.3.1 Ogden Model

The Ogden form which is an another phenomenological model, is directly based on the principal stretch ratios rather than the strain invariants;

$$W = \sum_{i=1}^{N} \frac{\mu_i}{\alpha_i}(\bar{\lambda}_1^{\alpha_i} + \bar{\lambda}_2^{\alpha_i} + \bar{\lambda}_3^{\alpha_i} - 3) + W = \sum_{i=1}^{N} \frac{1}{d_i}(J-1)^{2i} \qquad \text{Eq. [4.14]}$$

Where the initial bulk (μ_0) and shear modules (κ_o) are defined as;

$$\mu_0 = \frac{\sum_{i=1}^{N} \mu_i \alpha_i}{2}$$
$$\kappa_o = \frac{2}{d_1} \qquad \text{Eq. [4.15]}$$

μ_i, α_i, and d_1 are material properties defined by the user.

4.4.3.2 The Polynomial Form

The polynomial form is based on the first and second strain invariants. It is a phenomenological model of the form;

$$W = \sum_{i+j=1}^{N} c_{ij}(\bar{I}_1 - 3)^i(\bar{I}_2 - 3)^j + \sum_{k=1}^{N} \frac{1}{d_k}(J-1)^{2k} \qquad \text{Eq. [4.16]}$$

Where the initial bulk modulus (μ_0) and initial shear modulus (κ_o) are;

$$\mu_o = 2(c_{10} + c_{01})$$
$$\kappa_o = \frac{2}{d_1} \qquad \text{Eq. [4.17]}$$

Hyperelastic material constants c_{10}, c_{01} and d (material incompressibility parameter) are defined by user. These values can be derived from experimental test data.

ANSYS has lots of constitutive models for modeling hyperelastic materials with isotropic and anisotropic behaviors. In our simulations, two term Mooney-Rivlin model was used to express hyperelastic behavior of the tested material.

4.4.3.3 Two Term Mooney-Rivlin Model

This model is used in our studies for hyperelastic responses of tested materials. Mooney-Rivlin is the reduced form of the generalized polynomial equations of;

$$w = c_{10}(\bar{I}_1 - 3) + c_{01}(\bar{I}_2 - 3) + \frac{1}{d}(J-1)^2$$
$$d = \frac{(1-2\nu)}{(c_{10}+c_{01})} \qquad \text{Eq. [4.18]}$$

Hyperelastic Material Constants are c_{10} and c_{01} they characterize the deviatoric deformation of the material. In optimization and results section c_{10} and c_{01} are represented as C01 and C10 in ANSYS Parametric Design Language (APDL).

W = Strain energy potential
J = Determinant of the elastic deformation gradient F.
d = Material incompressibility parameter.
ν = Poisson's ratio is equal to 0.5 for incompressible materials.

4.4.4 Viscoelastic Material Finite Model for Tested Material

A material is said to be viscoelastic if the material has an elastic (recoverable) part as well as a viscous (non-recoverable) part. Upon application of a load, the elastic deformation is instantaneous while the viscous part occurs over time.

The viscoelastic model usually depicts the deformation behavior of glass or glass-like materials and may simulate cooling and heating sequences of such material. These materials at high temperatures turn into viscous fluids and at low temperatures behave as solids. Further, the material is restricted to be thermorheologically simple, which assumes the material response to a load at a high temperature over a short duration is identical to that at a lower temperature but over a longer duration. The material model is available with the viscoelastic elements for small deformation viscoelasticity and elements for small as well as large deformation viscoelasticity.

4.4.4.1 Constitutive Equations

A material is said to be viscoelastic if its stress response is made up of an elastic and viscous part. In a uniform load, indenter penetrates to tested material in experimental data; elastic region is instantaneous while the viscous region takes place over time. Viscoelastic material's stress function is usually described in integral form. Small strain theory for isotropic viscoelastic material can be shown below [24]:

$$\sigma = \int_0^t 2G(t-\tau)\frac{de}{d\tau}d\tau + I\int_0^t K(t-\tau)\frac{d\Delta}{d\tau}d\tau \qquad \text{Eq. [4.19]}$$

Where;

σ = Cauchy stress
e = deviatoric part of the strain
Δ = volumetric part of the strain
G(t) = shear relaxation kernel function
K(t) = bulk relaxation kernel function
t = current time
τ = past time

I = unit tensor

Note: The kernel function of f is taken to be any of the corresponding partition of the domain in finite elements solutions.

Integral form of the kernel functions of the generalized Maxwell elements for the viscoelastic elements:

$$G(t) = G_\infty + \sum_{k=1}^{N} G_k e^{(-t/\tau_k)}$$

$$K(t) = K_\infty + \sum_{k=1}^{N} K_k e^{(-t/\tau_k)} \qquad \text{Eq. [4.20]}$$

$$K(t) = K_\infty + \sum_{k=1}^{n_K} K_k e^{(-t/\lambda_k^K)} \qquad \text{Eq. [4.21]}$$

$$G_k = C_k(G_0 - G_\infty) \qquad \text{Eq. [4.22]}$$

$$K_k = D_k(K_0 - K_\infty) \qquad \text{Eq. [4.23]}$$

Where;

t = pseudo or reduced time

G(t) = shear relaxation kernel function

K(t) = bulk relaxation kernel function

n_G = number of Maxwell elements used to approximate the shear relaxation

n_K = number of Maxwell elements used to approximate the bulk relaxation

C_k = constant associated with the instantaneous response for shear behavior

D_k = constant associated with the instantaneous response for bulk behavior

G_0 = initial shear modulus

G_∞ = final shear modulus

K_0 = initial bulk modulus

K_∞ = final bulk modulus

λ_k^G = constant associated with a discrete relaxation spectrum in shear

λ_k^K = constant associated with a discrete relaxation spectrum in bulk

Stress response of viscoelastic materials is described by shear relaxation function G(t), it is represented in terms of Prony series, as below;

$$G(t) = G_\infty + \sum_{k=1}^{N} G_k e^{(-t/\tau_k)} \qquad \text{Eq. [4.24]}$$

Where;

G_∞ = long term shear modulus

G_k = shear elastic moduli, the coefficient of the Prony Series

τ_k = relaxation times for each Prony component, the other coefficient of the Prony Series

For ANSYS short term representation and two term Prony series, equation can be written as ; N=2

$$G(t) = G_0[\alpha_\infty + \sum_{k=1}^{2} \alpha_k e^{(-t/\tau_k)}] \qquad \text{Eq. [4.25]}$$

The coefficients τ_1 and τ_2 are same as equation [4.25] and represented as T01 and T10 in optimization and results sections, and they are also α_1 and α_2 are relative moduli and represented as A01 and A10 in ANSYS Parametric Design Language (APDL).

The coefficient of the Prony series (N) is taken two, like as in hyperelastic two terms Mooney - Rivlin method. It was taken from experimental force relaxation data using the small deformation assumptions from equation given below. It is

related about the solution effective shear modulus G for small indentation of rigid indenter.

$$G = \frac{3F}{16\delta\sqrt{R\delta}} \qquad \text{Eq. [4.26]}$$

Where;

F = force

δ = indentation depth of a rigid sphere

R = radius of rigid indenter of small indentation

4.4.5 Contact and Friction

Contact means two separate surfaces touching each other in such a way, that they become mutually tangent. Contact is a changing-status in non-linearity. That is, the stiffness of the system depends on the contact status, whatever parts are touching or separated.

Contact is a very important variable in finite element modeling. Face-to-face contact is automatically created by ANSYS when model is created in simulation. But in the model, some small overlaps or gaps appear, due to the contact regions between indenter and material. By giving slider tolerance, contact detection between bodies was tightening. To avoid divergence, tolerance value must be given correctly and gap between materials must be close to zero value.

Our model is frictionless in a manner of surface body to surface body frictionless contact. It means that, there is no friction effects and whole body 1 named as “indenter” in touch with other whole body named as “doku_int”. So, indenter completely penetrates to tested material.

The difficulty in the contact area is selecting correct contact settings where materials can move relatively to each other. Our model is frictionless because of non-linearity and the area of contact may change by loading.

Our model has standard unilateral contact, in separation normal pressure equals to zero. It only applies to regions of selected faces. Gaps which are related with tolerance can form in the model depends on loading. Model must be well constrained with frictionless type, weak springs with low k value are integrated into simulation in order to help to stabilize the model, to get a reasonable solution with flexible dynamic and optimization. Contact is symmetric. This means that the contact surfaces are constrained from penetrating the target surfaces and the target surfaces are constrained from penetrating the contact surfaces. Lagrange formulation actually supports symmetric behavior.

4.4.5.1 Theory of Contact in ANSYS

In ANSYS, physical contacting bodies do not interpenetrate. Therefore, the program must establish a relationship between the two surfaces to prevent them from passing through each other in the analysis. When the program prevents interpenetration, it enforces contact compatibility. There are different contact algorithms to enforce compatibility at the contact interface.

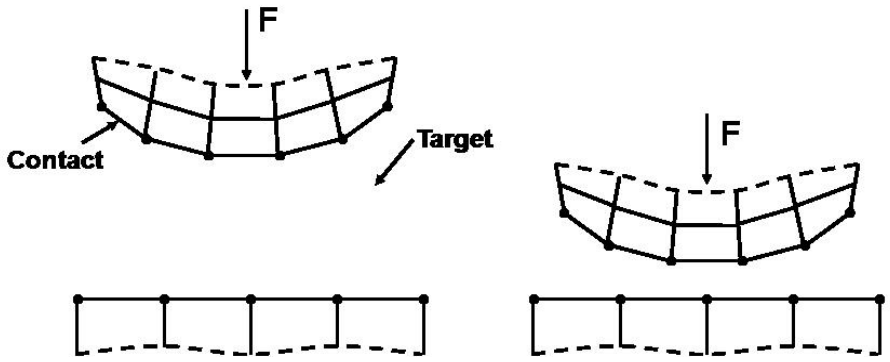

Figure 4.6 Contact Region [24]

For nonlinear solid body contact of faces, Penalty or Normal Lagrange formulations can be used. Both of these are penalty-based contact formulation and the formulation for contact comes from;

$$F_{normal} = k_{normal} x_{penetration} \quad \text{Eq. [4.27]}$$

Here,

F_{normal} : Finite contact force

k_{normal} : Concept of contact stiffness

$x_{penetration}$: penetration

The higher the contact stiffness and the lower the penetration are shown below. Ideally, for an infinite k_{normal}, one would get zero penetration. This is not numerically possible with penalty-based methods, but as long as $x_{penetration}$ is small or negligible, the solution results will be accurate.

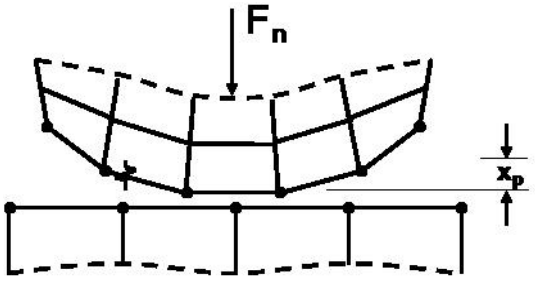

Figure 4.7 Penetration [24]

The main difference between Penalty and Lagrange methods is an extra term the contact force calculation;

Penalty: $F_{normal} = k_{normal} x_{penetration}$ Eq. [4.28]

Lagrange: $F_{normal} = k_{normal} x_{penetration} + \lambda$ Eq. [4.29]

Because of the extra term λ, the Lagrange method is less sensitive to the magnitude of the contact stiffness k_{normal}. The normal contact stiffness k_{normal} is the most important parameter affecting both accuracy and convergence behavior. A large value of stiffness gives better accuracy but the problem may become more difficult in terms of convergence and if the contact stiffness is too large, the model may oscillate with contacting surfaces bouncing of each other.

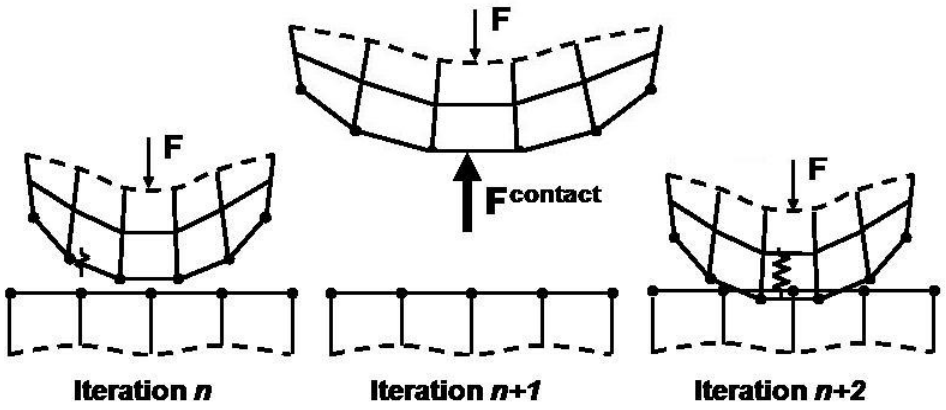

Figure 4.8 Iteration [24]

The default normal stiffness of model is automatically determined by simulation.

Contact formulation controls the underlying formulation for model, Normal Lagrange method was used to solve contact algorithm. Normal Lagrange enforces zero penetration when contact is closed making use of a Lagrange multiplier on the normal direction and a penalty method in the tangential direction [23].

Lagrange multiplier algorithm adds an extra degree of freedom (contact pressure) to satisfy contact compatibility. Consequently, instead of resolving contact force as contact stiffness and penetration, contact force is solved for explicitly as an extra DOF. Lagrange algorithm enforces the model to zero/nearly-zero penetration with

pressure DOF. It does not require normal contact stiffness but requires direct solver, which can be more expensive in terms of computability.

Chattering is an issue, which often occurs with Normal Lagrange method. If no penetration is allowed (Figure 4.9 left), than the contact status is either open or closed, and called as step function. This can sometimes make convergence more difficult, because contact points may oscillate between open/closed status. This possible oscillation is called chattering. If some slight penetration is allowed (Figure 4.9 right), it can make easier to converge, since contact is no longer a step change.

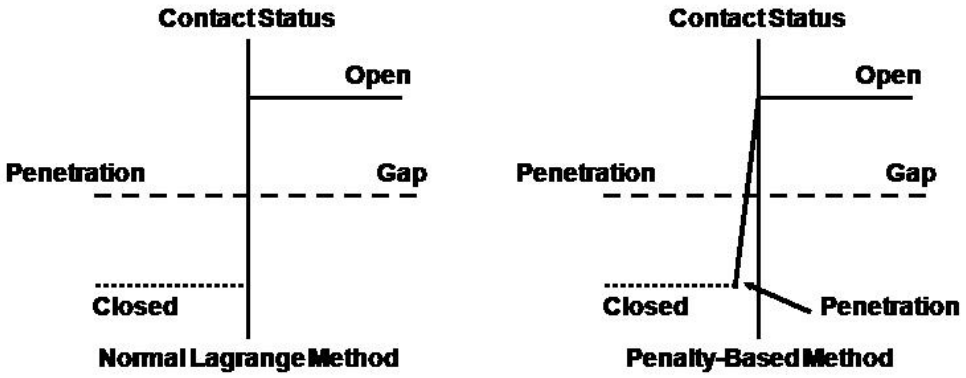

Figure 4.9 Chattering

Contact traction has been added to the model for extra degrees of freedom to required additional iterations, to control contact algorithm. When we compare Lagrange method with penalty method it is observed that, penalty method is not suitable for flexible – time dependent solution. In penalty method solution bases on end state such that it solves contact algorithm in model, it had already deformed before indenter go into tested material. However in Lagrange method, it solves contact algorithm step by step due to given time. Lagrange multiplier formulation is used in the normal direction while penalty-based method is used in the tangential direction.

Comparison of Penalty Method and Lagrange Method;

Table 4.2 Comparison of Penalty Method and Lagrange Method

Penalty Method		**Normal Lagrange Method**	
+	Good convergence behavior (few equilibrium iterations)	-	May require additional equilibrium iterations if chattering is presents
-	Sensitive to selection of normal contact stiffness	+	No normal contact stiffness is required
-	Contact penetration is present and uncontrolled	+	Usually, penetration is near-zero
+	Useful for any type of contact behavior	+	Useful for any type of contact behavior
+	Either Iterative or Direct Solvers can be used	-	Only Direct Solver can be used
+	Symmetric or asymmetric contact available	+	Asymmetric contact only
+	Contact detection at integration points	+	Contact detection at nodes

4.4.5.2 Thermal Conductance

Thermal conductance is a value for thermal contact conductance used in model and controlled by the program. However, in force relaxation experiment, finite element simulation and optimization, there is no temperature effect and heat exchange. All the experiments were done at room temperature.

4.4.5.3 Offsets

ANSYS Interface Treatment implies how the contact algorithm interface for the pair is treated. Model "Add Offset, Ramped Effects" was selected for adding additional defined offset values. It is a very close adjustment upon the default contact setting. "Add offset, ramped effects" applies the interface gradually over several sub steps within a load step. This selection does not close gaps, it creates small contact offsets to set the materials into initial contact algorithm. This can be used and fit in only nonlinear materials. There is no offset value in contact simulation. Identically to force relaxation experiment, in each time step, contact algorithm is changing and geometry is gaining new shapes related to intender positions and non-linearity. Time step controls offer an additional layer of convergence enhancement that allows bisections and adjustments to time step size based on changes in contact behavior.

4.4.5.4 Pinball Region

Pinball provides computational efficiency in contact calculations. Differentiation of the pinball region differentiates in open contacts and helps searching of which possible elements can contact with each other in a given contact region. It determines the amount of allowable gap for bonded contact and determines the depth at which initial penetration will be resolved if present.

The pinball region can be thought of as a sphere surrounding each contact detection point. If a node on a target surface is within this sphere, model simulation considers it to be in near contact and will not monitor its relationship to the contact detection point detailed. Nodes on target surfaces outside of this sphere will not be monitored closely for the particular contact detection point.
In Pinball region, contact search size can be adjusted. Commonly usage area is two contact bodies with large distances. In these cases pinball region must be increased. And another usage area is surfaces with the large deformation. Our model has large

deformation and requires residual over penetration. For this reason pinball region is used and controlled by program.

4.4.6 Meshes

Meshing is performed to perform discretion on the geometry created into small pieces called elements or cells. The purpose of this process can be explained in a straightforward and a logical manner. Engineering finite model is expected to be complex and it is impossible to solve it with whole model simulation. If the problem domain can be divided or meshed into smaller element set of grids or noted the solution within an element can be approximated [2]. Mesh generation is a very important task in the pre-process of tested material modeling. The tested material model has to be meshed properly into elements of specific shapes and the connectivity of meshed elements has to be established properly.

The common mesh type is triangulation and it is the most flexible and well-established type. It can be used for two and three dimensional models. It grants flexibility in modeling complex geometry and its boundaries. But accuracy of simulation results is often lower than quadrilateral elements.

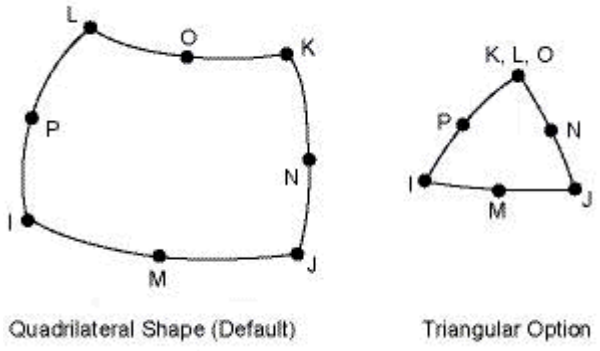

Figure 4.10 Different Types of Meshes [2]

With quadrilateral elements, simulation of models is more accurate and realistic. The deformation of the model can be seen more easily and the force relaxation calculations for large deformations are more suitable. However, it is more difficult to generate automatic meshing for complex materials. But in our model quadrilateral elements were used and tested material was meshed by manually and size of the meshes was given by user. By doing this, more accurate and suitable meshes were created in our model.

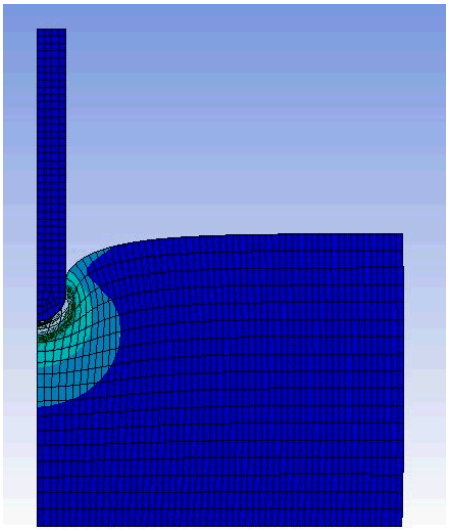

Figure 4.11 Meshes

ANSYS program uses its default mesh control algorithm. In automatic mesh control, user will not need to specify and control mesh. But due to our model's properties, large deformations and viscoelastic behavior need specific meshes for the solutions to be converged. Mesh controls allow user to establish such variables as the element shape, node placement of meshes and element properties to be used in meshing the solid model [23]. Using mesh tool in ANSYS, the mesh parameters are changed and optimal mesh created;

- Element Shape
- Element Size
- Meshing Type (free or mapped)

- Controlling Smart sizing level

In ANSYS, user must choose physics preferences of meshes. It is based on the physics of the analysis type. There are four types that user can set:

- Mechanical
- Electromagnetic
- CFD
- Explicit

In the simulation, mechanical type was selected because of the required meshes for mechanical analysis. They are the patch for conforming meshes to provide robust, easy to use meshing tools and it will simplify the mesh generation tools.

By using relevance of the model, user can control the finesses of the mesh for all simulations. Changing the value for relevance to minus values (-100) it gets high speed solutions or changing it to positive values (+100) it gets more accurate solutions. In this study for simulations, the value of relevance was set to zero and relevance center was selected as coarse.

Another important adjustment in meshing is shape checking. It ensures a quality mesh based on specific error limits. “Standard Mechanical” was selected in the model and it uses the default Workbench shape criterion. This selection has proven to be effective for nonlinear problems. In standard mechanical simulation, a unitless metric is used to compare volume to edge elements. Jacobian ratio was used for this purpose. If the Jacobian ratio is less than 0 or greater than the limit, then the metric is -1.0 and will cause shape failure. Jacobian ratio is computed at integration points [23].

An additional adjustment for mesh sizing is Initial Size Seed of the model. It is an active assembly and program can control initial seeding of the mesh size for each part. It bases on the initial seeding and the mesh of simulation. It will be changed by

suppressed and unsuppressed parts because of the bounding box's growing and shrinking conditions. These conditions are related with smoothing of mesh elements.

The smoothing selection attempts to improve element quality by moving location of the nodes with respect to surrounding nodes and elements. Medium smoothing was selected and transition is slow that affects the rate at which adjacent elements will grow.

The sizing control is the last parameter for meshing. User must select element size for each model in simulation and the size for selected body will be body, face or edge. In our model to simulate experimental data, we have used face and edge sizing. All the element sizes were given manually and tuned to set up a converge solution.

For flexible bodies, the mesh density is based on the following

- The mesh should be fine enough to capture mode shape of the structure.
- If the stresses and strains are of interest, the mesh should be fine enough to capture these gradients accurately.

4.5 Flexible Dynamic Analysis

As mentioned before, all experiments were done by time based and step by step iteration. In finite simulation of experiments, all time steps must be checked smoothly and carefully, so dynamic formulation for modeling must be used to get simultaneous data. For this reason flexible analysis was used in ANSYS to model simulations.

Typically the model is connected in such a way that it forms a mechanism that can be driven by force or displacement. The response will be based on the kinematic of

the mechanism and in the case of a force loading it will be based on the inertia of the parts. A flexible analysis may consider rigid or flexible bodies. The displacements and rotations are due to joints and also due to flexible part deformations.

The advantages of flexible analysis;

- Bodies can be flexible
- All nonlinearities supported
- All boundary conditions supported
- Surface to surface contact between bodies can be included
- Rigid or flexible can be used on a part by part base

The models in flexible analysis can use ANSYS elements. Bodies are connected by joints and they interact at their surfaces. Flexible bodies may contain material nonlinearities. In flexible analysis the initial velocity of the bodies is assumed to be zero, but a constant non-zero initial velocity can also be specified. The result of typical analysis has animation of model motion, maximum and minimum displacement, velocity and acceleration. Forces, moments and relative motions at joints can be observed. Briefly, flexible analysis must be used to include flexible bodies, surface contacts, nonlinearities and boundary conditions. For our model, flexible dynamic gives perfect solution and with simulating all aspects of the analysis, 2D visualization of the model and motion shows the success of the analysis.

Flexible dynamic analysis provides user the ability to determine the dynamic response of the system under any type of time-varying loads. For flexible and non-linear materials such as our experimental material, stresses and strains can be considered as outputs. Flexible dynamic analysis is also known as time-history analysis or transient structural analysis.

Flexible dynamic analysis is needed to evaluate the response of deformable bodies when inertial effects become significant.

- If inertial and damping effects are ignored, a linear or nonlinear static analysis instead can be considered.
- If the loading is purely sinusoidal and the response is linear, a harmonic response analysis is more efficient.
- If the bodies can be assumed as rigid and the kinematics of the system is of interest, rigid dynamic analysis is more cost-effective.
- In all other cases, flexible dynamic analyses should be used, because it is the most general type of dynamic analysis

In a flexible dynamic analysis, ANSYS Workbench solves the general equation of motion

$$[M]\{\ddot{x}\}+[C]\{\dot{x}\}+[K(x)]\{x\}=\{F(t)\} \qquad \text{Eq. [4.30]}$$

Applied loads and joint conditions may be a function of time. As seen above, inertial and damping effects are now included. Hence, the user should include density and damping in the model. Nonlinear effects, such as geometric, material and/or contact nonlinearities are included by updating the stiffness matrix. Flexible dynamic analysis encompasses static structural analysis and rigid dynamic analysis and it can be used for all types of connections, loads and supports. However, one of the important considerations of performing flexible dynamic analysis is the time step size:

- Time step should be small enough to correctly describe the time-varying loads.
- The time step size controls the accuracy of capturing the dynamic response.
- The time step size also controls the accuracy and convergence behavior of nonlinear systems.

During flexible dynamic analysis, automatic time-stepping is used in our study. Because of the proper selection of the initial, minimum, and maximum time steps are important part of the representation of the dynamic response with related high accuracy. Unlike rigid dynamic analysis which uses explicit time integration, flexible dynamic analysis uses implicit time integration. Hence, the time steps are usually larger in flexible dynamic analysis. The dynamic response can be thought as various modeshapes of the structure being excited by a loading. The initial time step should be based on the modes (or frequency content) of the system.

As a general suggestion for the selection of the initial time step t_1 the following equation can be used;

$$\Delta t_{initial} = \frac{1}{20 f_{response}} \qquad \text{Eq. [4.31]}$$

Where $f_{response}$ is the frequency of the highest mode of interest.

In order to determine the highest mode of interest, a preliminary model analysis should be performed prior to the flexible dynamic analysis. In this way, the user can determine what the mode shapes of the structure and the value of $f_{response}$.

The automatic time-stepping algorithm will increase or decrease the size of the time step during the course of the analysis based on the calculated response frequency.

- Automatic time-stepping algorithm still relies on reasonable values of initial, minimum and maximum time steps.
- By using minimum time step, simulation's initial time steps will be too large.

When performing a model analysis to determine an appropriate response frequency value, it is not sufficient to request a certain number of node to use the maximum frequency. It is a good idea to examine the various model shapes to determine which frequency may be the highest mode of interest contributing to the response of the structure.

For flexible analysis of non-linear materials appropriate properties such as density, Young's Modulus and Poisson's ratio has to be considered and non-linear materials such as viscoelasticity and hyperelasticity must also be included. As mentioned above, two term Mooney-Rivlin model based on strain invariants is selected for hyperelasticity and also it is included in ANSYS database and two term Prony Series for viscoelasticity defined with external algorithm based on shear relaxation function coded to ANSYS.

"Step controls" is another important specification for solution of simulation time algorithm. It allows user to control time step size in a transient analysis. The number of steps controls how the load is divided. The "step end time" is the actual simulation ending time for all step number in simulation. In model, step ending time was used as 30 seconds.

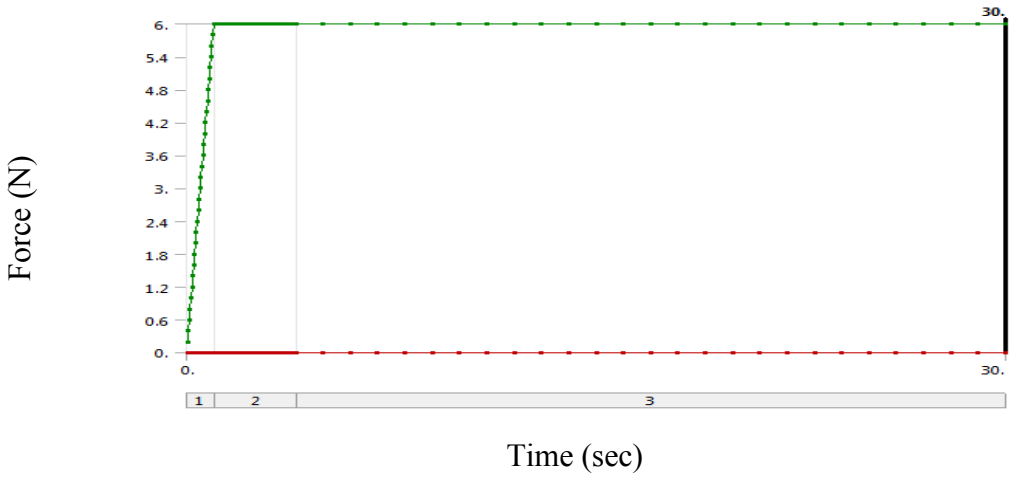

Figure 4.12 Time Steps

As seen above Figure 4.12, when modeling the experiment, three steps were used. First step in the experiment is the penetration of indenter to tested materials. This period takes one second. Column of the figure is depth of the penetration in millimeters.

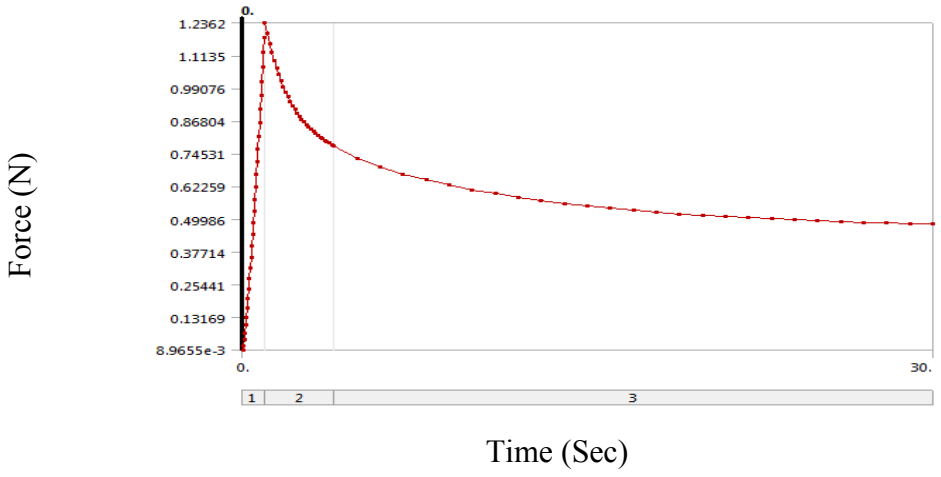

Figure 4.13 Force Reaction Graph

Second step is between second and fourth seconds; here, tested material's stress relaxation is changing and decreasing rapidly. There are lots of iterations in this step and they must be considered carefully in these three seconds because of viscoelastic and hyperelastic behaviors. After that, the last step comes and it takes 26 seconds. It is related with creep deformation and hysteresis of material and it gives stable stress relaxation values (counter forces) to the intender.

The "solver controls" section allows the user to choose the equation solver. This section is for the use of weak springs and use of large deflection effects. Flexible dynamic analysis may typically involve large deformations, so "Large Deflection" must be added to model. Also in the case of large deflection we usually turn on weak springs.

Output control allows users to control how frequently data is saved to the ANSYS result file. For multiple step analysis, once can save results only at the end of the step. One can also save results at intervals that are as evenly-spaced as possible (depending on automatic time-stepping).

Converge Criteria**;** When solving nonlinear static or transient analysis an iterative procedure (equilibrium iterations) is carried out at each substep. Successful solution is achieved when the out-of-balance loads are less than the specified convergence criteria. Criteria appropriate for the analysis type and physics are displayed in this grouping [23].

4.6 Commands

In commands tree, user can use ANSYS or APDL codes upon the selected simulation. With use of ANSYS Parametric Design Language (APDL), deterministic method capabilities, sensitivities, design, analysis graphs and optimization can be done.
For optimization, specific command setup, which contains APDL, about optimization has been added to model tree. With added codes, user can identify input and response parameters from the APDL Parameters list and send them to DesignXplorer where all the optimization process can be completed. Coded APDL and their explanations can be observed below,

All the APDL explanations are taken from ANSYS Help

Commands inserted into this file will be executed just prior to the Ansys SOLVE command.

! These commands may supercede command settings set by Workbench.

! Active UNIT system in Workbench when this object was created: Metric (mm, kg, N, C, s, mV, mA)

/PREP7; Preprocessor to build the model (geometry, materials, etc.)

$$C01 = 0.003426$$
$$C10 = 0.003426$$
$$T1 = 1.0$$
$$T2 = 9.0$$
$$A1 = 0.393$$
$$A2 = 0.266$$
$$D = (1\text{-}2*0.49)/(C01+C10) \qquad \text{Eq. [4.32]}$$

Initial values;

C01 and C10 = Hyperelastic material coefficients as a result of two term Mooney-Rivlin Model

T1, T2, A1 and A2 = Viscoelastic material coefficients as a result of two term Prony Series

D = Material incompressibility parameter

$$d = \frac{(1-2v)}{(c_{10}+c_{01})} \qquad \text{Eq. [4.33]}$$

v = Poisson ratio and is equal to 0.5 for incompressible materials.

All initial values were taken from estimated material properties of pig #2 [1].

CMSEL,S,doku,ELEM ;

CMSEL = Selects a subset of components and assemblies

S = Select a new set

ELEM = Specifies “Elements” as the subsequent status topic.

By this, “doku” component/ material was selected. It was created in material selection tree in ANSYS and dedicated to tested material.

ESLN,S

ESLN = Selects those elements attached to the selected nodes.
S = Select a new set

All the elements in “doku” were selected by this comment.

TB,HYPE,3,1,2,MOON

TB = Activates a data table for nonlinear material properties or special element input.
HYPE= Hyperelasticity
MOON = Mooney Rivlin Model

Selected three materials, assisted as a hyperelastic material with two term Mooney-Rivlin model.

TBTEMP,0

TBTEMP = defines a temperature for the data table.

Temperature must be added to solve algorithm and considered as zero.

TBDATA,,C10,C01,D,

TBDATA = Defines data for the data table.

The coefficients for the hyperelastic model were identified as input parameter for DesignXplorer.

TB,PRONY,3,1,2,SHEAR

PRONY = Prony Series
SHEAR = Viscoelasticity behavior

Selected number three material, assisted as a viscoelastic material with two term Prony series.

TBTEMP,0

Same as above.

TBDATA,,A1,T1,A2,T2,,

The coefficients for the viscoelastic model were identified as input parameter for DesignXplorer.

MP,EX,3,0.015
MP,EY,3,0.015
MP,PRXY,3,0.49

MP = Defines a linear material property as a constant or a function of temperature.
EX = Estimated Elastic modulus in X (Pa)
EX = Estimated Elastic modulus in X (Pa)
PRXY = Poisson's Ratio

Required data are given to model for material properties.

EMODIF,ALL,MAT,3

EMODIF = Modifies a previously defined element
MAT = Material

Modify all selected elements as a material three

CMSEL,ALL
ALLSEL,ALL

All material's components and elements are selected as to get converge solution. In case of having any missing elements will cause divergence problem.

finish

Finish the APDL comments.

/SOLU

It specifies solution summary data per sub-step to be stored. And it is ready for APDL Parameters menu to solve optimization.

After that ANSYS input file was created to insert new commands for optimizations between force reactions of tested material and simulated model. In the end optimization algorithm minimizes the error of objective functions. Therefore, error must be a response parameter of optimization. Relaxation graph of the tested material was drawn. The force reactions changing by time were also calculated. A file whose name is "test" has been created in order to perform optimization process.

In below, additional code and their exploitations can be seen;

**DIM,arrays,ARRAY,86*

A vector named arrays was created with 86 rows.

**VREAD,arrays(1),Test*

Program reads 86 points from test whose created before and assigned to array.

(1F6.1)

It is related with format of test file.

/post1

It activates the post processing menus.

SET,FIRST

Algorithm calls the first (initial) finite solution from its solution file.

sum2 = 0

sum2 value equals to zero.

**do,i,1,86*

It repeats solution for all 86 steps.

CMSEL,S,fixed,NODE

The fixed component from ANSYS workbench is selected. The component consists of nodes but the nodes are not in any order.

**get,nodenumber,node,,count*

It gets the number of nodes from selected set of nodes.

sum = 0

sum value equals to zero.

**do,j,1,nodenumber-1*
**get,nodenum,node,,num,max*

It selects the minimum node number from set of nodes.

**get,reactionf,NODE,nodenum,RF,FY !*

It gets the reaction force for the selected node.

sum = sum + reaction

By using this algorithm, all the reactions on direction y are added, so total reactions of y direction can be calculated.

nsel,u,node,,nodenum

.

It deselects nodes which were already selected previously, disallowing same node to reenter the loop.

**enddo*

End of the loop.

sum2 = sum2 + (arrays(i)-sum)(arrays(i)-sum)*

After finding all reaction forces, for a specific step, the algorithm subtracts test data's values form finite model's values and takes square of it. The total of the

errors give least square error. In optimization chapter, the error and optimization type discussed more detailed.

SET,NEXT

Algorithm goes to other solution step.

CMSEL,ALL

Select all the components.

ALLSEL,ALL

All the materials have to be selected for getting a converge solution. Any missing element should cause divergence problem.

RF = sum2

sum2 equals to RF.

Least square error is expressed as RF. It is the response parameter of APDL Parameters. Optimization of the model is constructed which is based on least square error. The main goal is reducing least square error by using optimization methods of ANSYS.

CHAPTER 5

OPTIMIZATION

In modern science, the process of optimization is used to maximize or minimize values for a model at hand, which are originally limited or constrained to some constant values by its user, hence resulting in the pickup of the most suitable element from the eligible alternatives.

In our studies DesignXplorer tool is used for optimization. DesignXplorer environment helps user to associate parameters to APDL. User can create design and analysis graphs, take the advantage of deterministic method capability, make optimization and adjust sensitivities by using ANSYS APDL input files.

As mentioned above, this process is used for enhancing initial value of the model to a more optimum one, and during this enhancement, hyperelastic and viscoelastic coefficients and compressibility parameters are used for reference data, where the output (response) parameters correspond to error function.

"The optimization algorithm minimizes the objective function by using least square error defined as; [1]"

$$Error = \sum_{j=1}^{M} (F_j^{EXP} - F_j^{FEM})^2 \qquad \text{Eq. [5.1]}$$

Where;

M = Number of data samples

F_j^{EXP} = Experimental force value of j^{th} sample

F_j^{FEM} = Force value obtained from the FEM solution of j^{th} sample

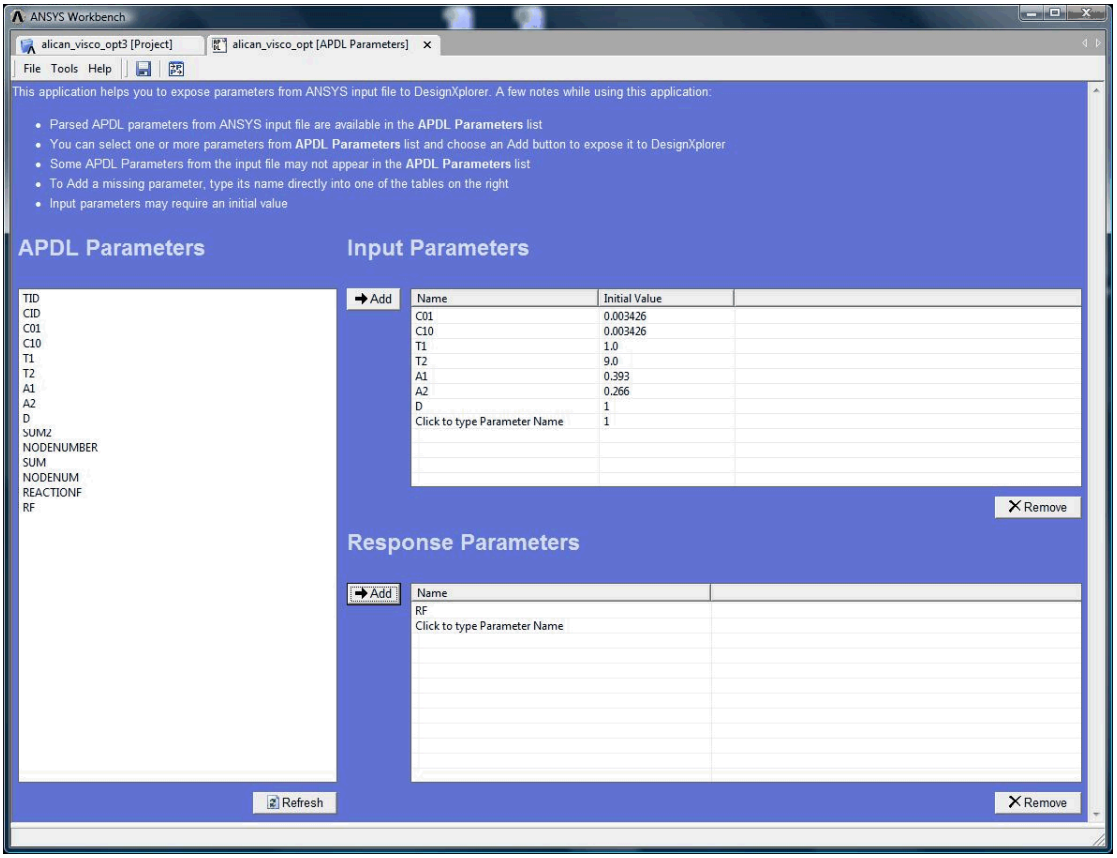

Figure 5.1 APDL Parameters

Before performing optimization step, APDL Parameters were selected and sent to application. Input parameters and their initial values were given to the solver whose screenshot is shown above. Response parameter RF and least square error function were selected as optimization criteria.

As mentioned in the introduction, an add-on is required upon ANSYS to enable more and better options for the user. As mentioned before, the DesignXplorer is an add-on tool of ANSYS where user can design analysis response of models. Design of Experiments (DOE) and other optimization methods are used for deterministic method and it is based on the given parameters. Response of surface and design sets can be calculated easily with use of goal driven optimization method.

5.1 Design of Experiments

Design of Experiments (DOE) is a method for collecting sampling point's locations. "In engineering literature, there are lots of design of experiments applications however all of versions try to locate the sampling points such that the space of random input parameters is explored in the most efficient way, or obtain the required information with a minimum of sampling points [23]." The required number of sampling points is reduced by efficient sample point detection. DOE combines a center point as a reference point and other points along the axis of the input parameters which are given by user. Points are determined by a fractional factorial design.

The finite element analysis depends on material properties. Each change in input response value results in a need for a new finite element analysis design in optimization, based on design of experiments. A response surface is drawn by ANSYS for solution, where the functions of finite elements are dependent to all selected input variables. In following sections, response surfaces of material coefficients, as are input parameters, are studied. The design of experiment method creates a new response surface by using curves and surface adjusting algorithms, to fit in the solutions. Individually, all solution of DOE has to be adjusted to response parameters. DOE is the most suitable solution of deterministic method for solving the tested material optimization because of above explained advantages.

Other solution methods, such as Variational Technology, Six Sigma Analysis and Robust Design could also be used. However, they are not suitable for solving the optimization problem, since it depends rather on optimization of input and output parameters.

5.2 Structure of DesignXplorer

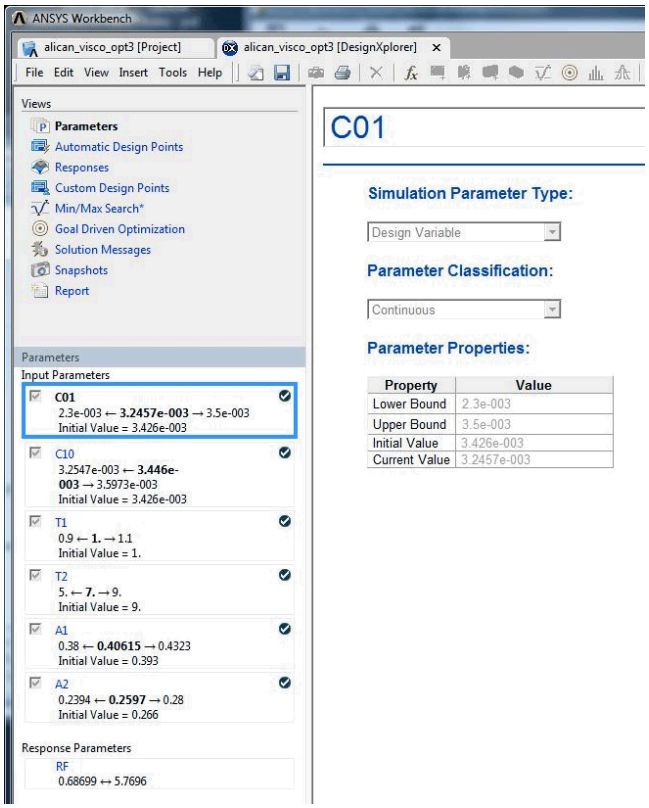

Figure 5.2 Structure of DesignXplorer

As discussed in previous sections, all optimization is made by DesignXplorer which is a powerful tool for designing and optimizing models in ANSYS.

5.2.1 Parameters

Previously set parameters are displayed in APDL Parameter section. When a parameter is selected, user can get all information about that parameter in the right

section of the panel. Certain parameters such as elastic modulus of the model defined in model affect some model properties however will have no effect on actual geometry, so there is no parameter selection part for them in DesignXplorer.

Another important parameter is input parameter's range. Range must be adjusted correctly, with respect to the input geometry. In our simulation, a default value of +/- 10 was used.

Input parameters (Viscoelastic and hyperelastic model coefficients) can be selected as either discrete or continuous values, and these selections have specific forms among themselves. Discrete parameters are not continuous in model, as for example in the fillet part of the model. "However continuous parameters can be selected any value defined by the range of user set [23]."

Response parameter "RF – Least square error" is the result which is derived from the output form of the analysis.

5.2.2 Automatic Design Points

Design Point is the snapshot of parameter values. All input and response parameters are included in the snapshot. Our model's Design Points are automatically created, while parameter values were calculated directly in simulation.

In deterministic method, the values of the automatic design points are verified according to design of experiment method (DOE). As mentioned before, design of experiment method is central composite design with a fractional factorial design. The generated automatic design points are calculated according to input and response parameters.

The upper and lower values of the DOE points are directly related with input variable in optimization. For goal driven optimization, DOE points must be close to

optimum design parameters. The suitable optimization for our model is using automatic design points and goal driven optimization with DOE method. This gives the best fitted and optimized input parameters by minimizing the response parameter RF (Error).

In DOE theory, response surfaces are generated in two steps;

- First, solving all response parameters for all automatic design points with given simulation constraints.

- Second, fitting the response parameters as a function of the input parameters which are created by using regression analysis techniques.

5.2.3 Responses

In this part, some response surfaces for every parameter in simulation are displayed, as 3-D Contour graphs. Min/Max Search helps user to examine the entire output parameters. It automatically comes with goal driven optimization and it is an actual search. Further and more detailed explanations and drawings regarding these responses are available in "Results" chapter.

5.2.4 Goal Driven Optimization

Multi-Objective Optimization is an effective method to achieve suitable and successful designs from a sample set, with its goals given before the user sets parameters. A sub-discipline of Multi-Objective Optimization is Goal Driven Optimization. In goal driven optimization, user can state a series of design goals, which will be used to generate optimized designs [23]. GDO and MMO processes allow the user to check the effects of given response parameters on given parameters with selection. Screening method is used to generate sample sets.

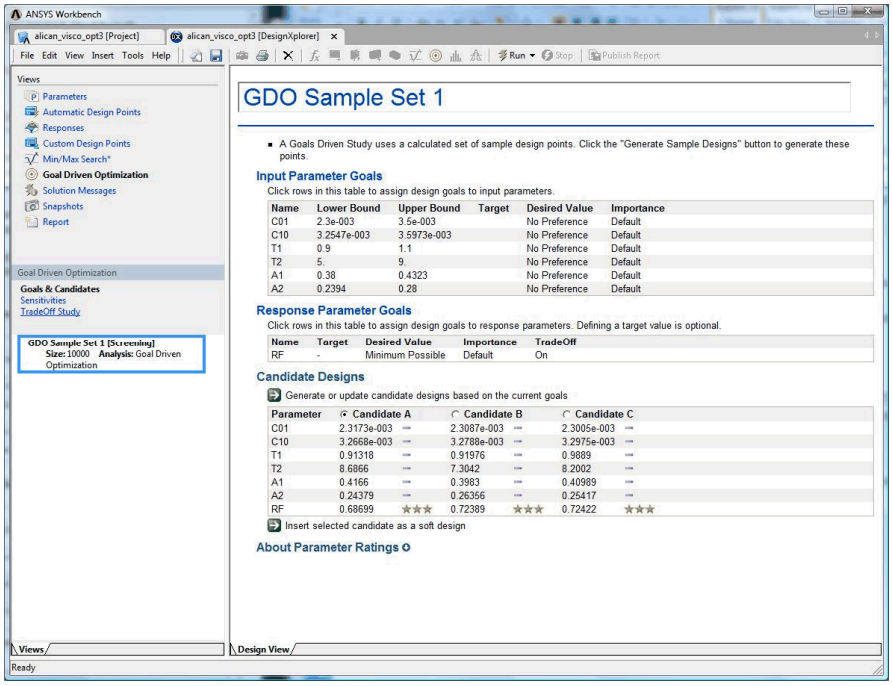

Figure 5.3 Goal Driven Optimization

The screening method is a non-iterative direct sampling method. It uses quasi-random generator based on the Hammersley algorithm. The advanced method which uses Multi-objective Genetic Algorithm is another method but it can only optimize continuous input parameters. Models with mixed parameter types and smooth diverge behavior must be solved with screening method. Screening method is used generally for preliminary design.

The Hammersley algorithm is based on radical inverse function. Any integer n can be represented as;

$$n = n_0 n_1 n_2 n_3 ... n_m$$

$$n = n_m + n_{m-1} * R + ... + n_0$$

$$\Phi_R(n) = 0 n_m n_{m-1} n_{m-2} ... n_0 \qquad n = n_0 n_1 n_2 n_3 ... n_m \qquad \text{Eq. [5.2]}$$

$$= n_m * R^{-1} + n_{m-1} R^{-2} + ... + n_0 * R^{-(m-1)}$$

$$H_k(i) = [i / N, \Phi_{R1}(i), \Phi_{R2}(i) ..., \Phi_{Rk-1}(i)]$$

In general, for a radix R representation for the equation;

$$n = n_m + n_{m-1} * R + ... + n_0 \qquad \text{Eq. [5.3]}$$

By reversing the order of the digits in equation above,

$$\Phi_R(n) = 0 n_m n_{m-1} n_{m-2} ... n_0$$
$$= n_m * R^{-1} + n_{m-1} R^{-2} + ... + n_0 * R^{-(m-1)} \qquad \text{Eq. [5.4]}$$

Thus, in k dimensional space, Hammersley points;

$$H_k(i) = [i / N, \Phi_{R1}(i), \Phi_{R2}(i)..., \Phi_{Rk-1}(i)] \qquad \text{Eq. [5.5]}$$

Where i=0,.., N indicates sample points.

Goal Driven Optimization method uses "Decision Support Process", a post processing action, which is based on a weighted aggregate method and creating Pareto fronts. In screening approach, the solutions of optimization are distributed across all the Pareto fronts.

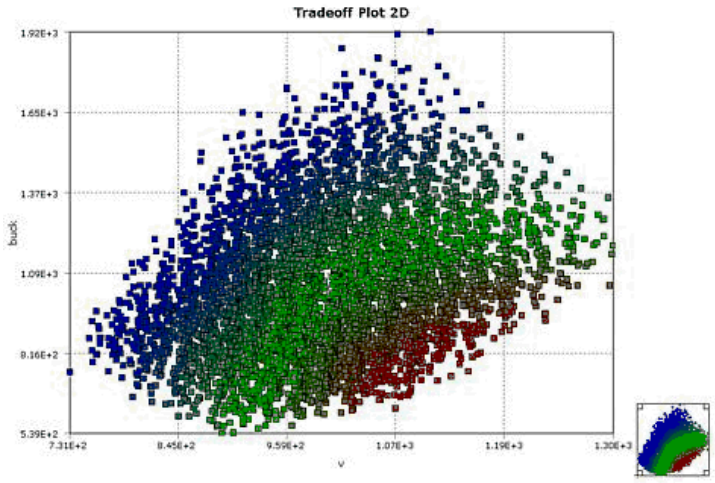

Figure 5.4 Sample Points Generated by Screening Method

Post-processing of Goal Driven Optimization in screening method is related with sample generation. It generates Pareto fronts by using the Decision Support Process to generate three candidate designs. From the candidates, user can pick up the most suitable optimized input parameters by checking error function. Three – dimensional plots are typical 3-D solution points with feasible and infeasible points.

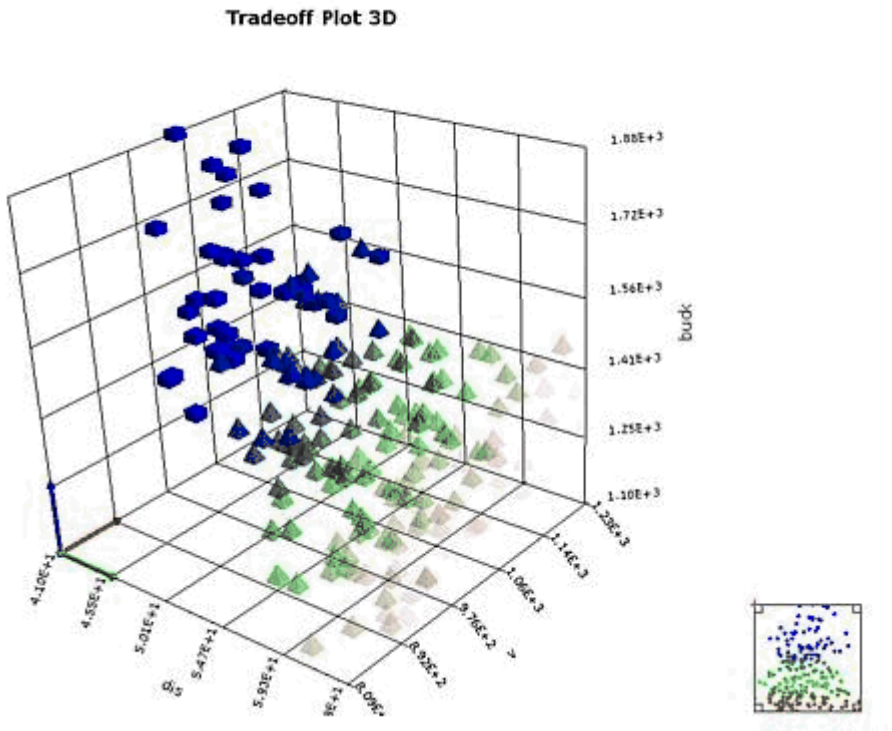

Figure 5.5 3-D Plots with Solution Points

The candidate with least error is the most suitable one for selection and this candidate's material coefficients have to be used for a new finite element analysis solution. It is called optimized model and it is also created by using inverse finite element method.

CHAPTER 6

RESULTS

In this chapter, results of finite element analysis (initial & optimized) and optimization are discussed. Many different stress relaxation tests were done during data collection process. For example, different materials (gel viscoelastic material, foam viscoelastic material, arm – soft tissue) and different penetration depths (6 mm, 8 mm, 10 mm) are used to collect experimental data. Experiments with different variables, give us different relaxation graphs. To understand and examine the process of analysis and optimization, gel viscoelastic material with 6 mm penetration is taken as an example.

The actions taken in this chapter are given step by step below,

1) Inverse Finite Element Solution with Initial Values: A model has been developed, with respect to the material coefficients in hand. After the model has been simulated, necessary graphs are plotted, and force reaction graph are chosen to be used as comparison graph.

2) Experimental Result: The data derived from stress relaxation tests and force Reaction Graph (Relaxation Graph) is processed by Low-Pass Filter, and used in optimization.

3) Optimization: The graph from the initial values is optimized upon the experiment data. The method of optimization is based on least square error, as mentioned in

previous sections, and since we take the square of error value, the error rate is very low. At the end of optimization, the calculated values are the material coefficients of the experimented material.

4) Optimized material coefficients are taken to be used in the new model. This model becomes the model of previously experimented material for stress relaxation graph.

5) Comparison of force reactions (Relaxation Graphs) of initial model with respect to optimized model, to observe how compatible and proper is the optimization due to experiments.

6.1 Inverse Finite Element Solution with Initial Values

First, material model with initial values was created in ANSYS. It is a viscoelastic & hyperelastic two model based material. The initial values and material models are discussed in previous sections. After solution of simulation, ANSYS gives solution graphs; (These graphs are initial value based graphs after optimization. In our study optimized graphs for our model are used).

- Total deformation graph (Figure 6.1)
- Equivalent stress graph (Figure 6.2)
- Equivalent elastic strain graph (Figure 6.3)
- Maximum principal elastic strain graph (Figure 6.4)
- Force Reaction graph (Relaxation graph) (Figure 6.5)

The important graph is force reaction for optimization and discussed detailed below.

Figure 6.1 Penetration Graph and Simulation for Initial Values

Figure 6.1 is related with indenter's movement. Indenter's position and penetration ratio can be checked for specific time. As mentioned before during experimental process, there are three main time stages. First time stage is penetration of indenter and it penetrates 6 mm to material in one second. Second stage is stress relaxation peak process and final step is stabilizing of force reaction in stress relaxation graph. Time stages' force reactions can be seen in Figure 6.5. In simulation figure indenter color is red because of penetration. Color line of simulation means the penetration depth. When the penetration takes place blue color is changing to red in model. In the simulation indenter color is the red because of its maximum penetration (maximum penetration 6 mm).

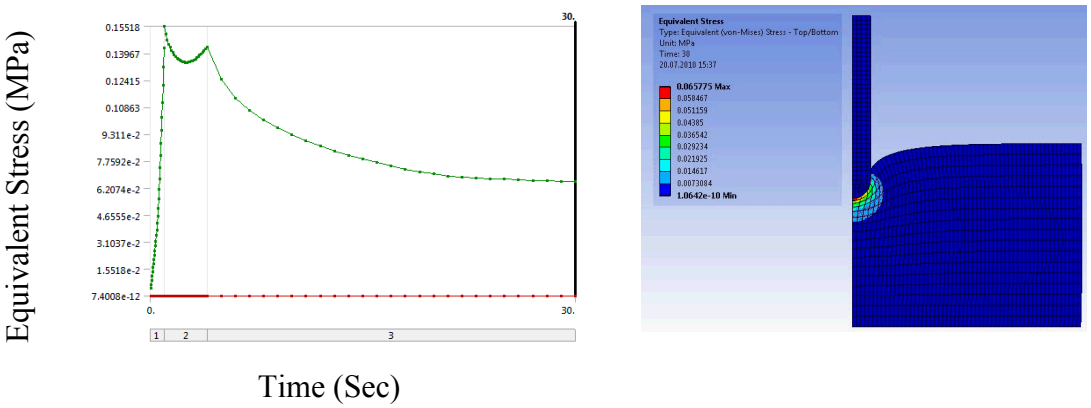

Figure 6.2 Equivalent Stress Graph and Simulation for Initial Values

Figure 6.2 is the Equivalent stress diagram of the model during experiment. This figure based on time and time steps. Equivalent stress changes according to time steps can be seen easily in figure. Simulation of model color line is same like others. It indicates the ratio of equivalent stress in terms of MPa. The equivalent stress distribution of model explained in simulation by colors. Maximum equivalent stress was observed in contact area between indenter and material.

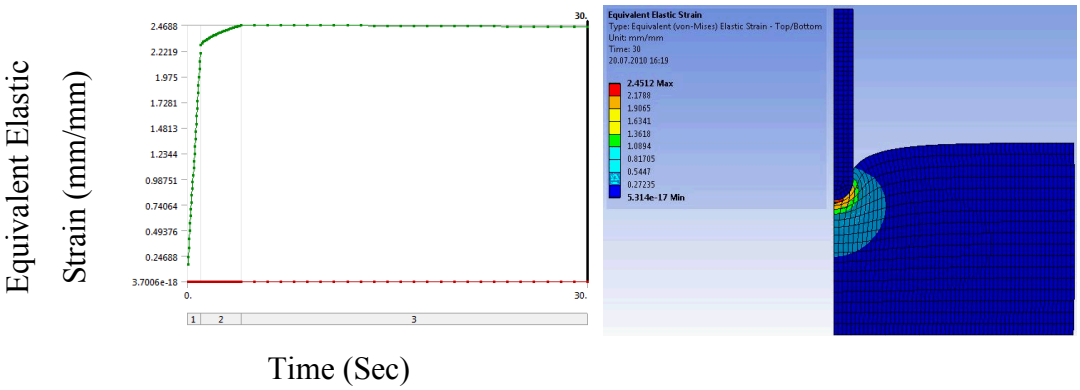

Figure 6.3 Equivalent Elastic Strain Graph and Simulation for Initial Values

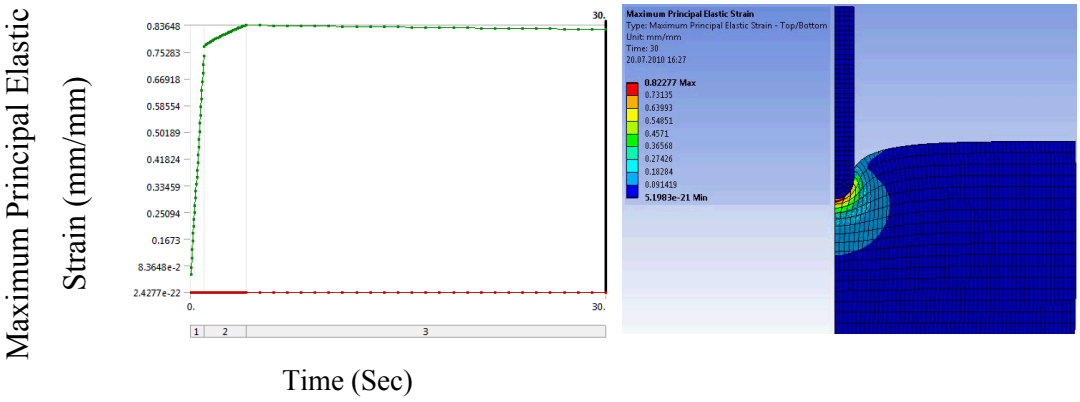

Figure 6.4 Maximum Principal Elastic Strain Graph and Simulation for Initial Values

Figure 6.3 and 6.4 are elastic strains. First graph and simulation is equivalent elastic strain in terms of mm/mm. And its simulation indicates the distribution of elastic

strain. Second graph is the maximum principal elastic strain and its simulation. The same color line specifies division of strain like other graph.

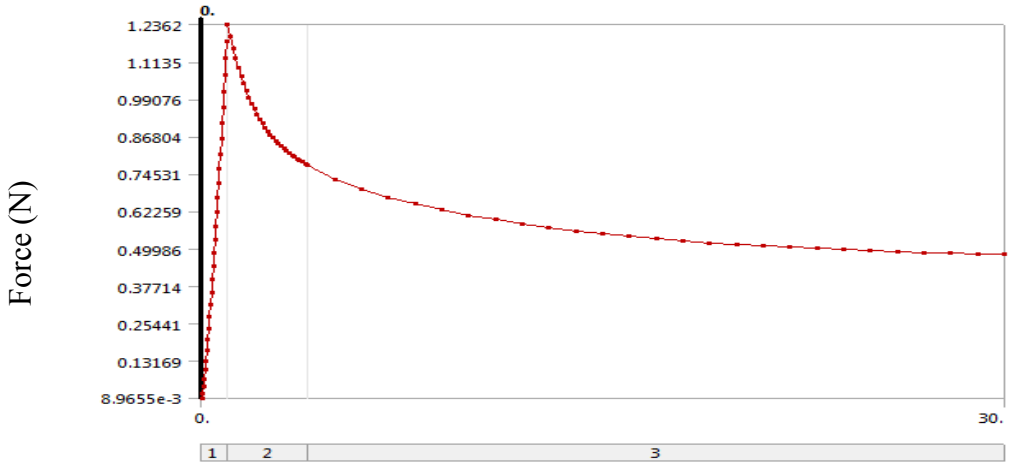

Figure 6.5 Force Reaction (Relaxation) Graph for Initial Values

Figure 6.5 shows the most important graph in our simulation. It is the reaction force (relaxation) graph which is given by simulated model to indenter in simulation. The initial values are used to simulate model so this graph is directly related with given hyperelastic and viscoelastic coefficients. ANSYS tries to fit and optimize this graph to given experimental data graph. By this way, we can find correct coefficients for tested material due to stress relaxation test and its data.

6.2 Experiment Results

Experiments, the raw data and filtering are discussed in Experimental Setup chapter. Figure 6.6 is the test data for gel material with 6 mm penetration. The raw data was filtered by Low-Pass filter and smoothed for graph. Optimized FEA model's force relaxation graph must be fitted to this graph.

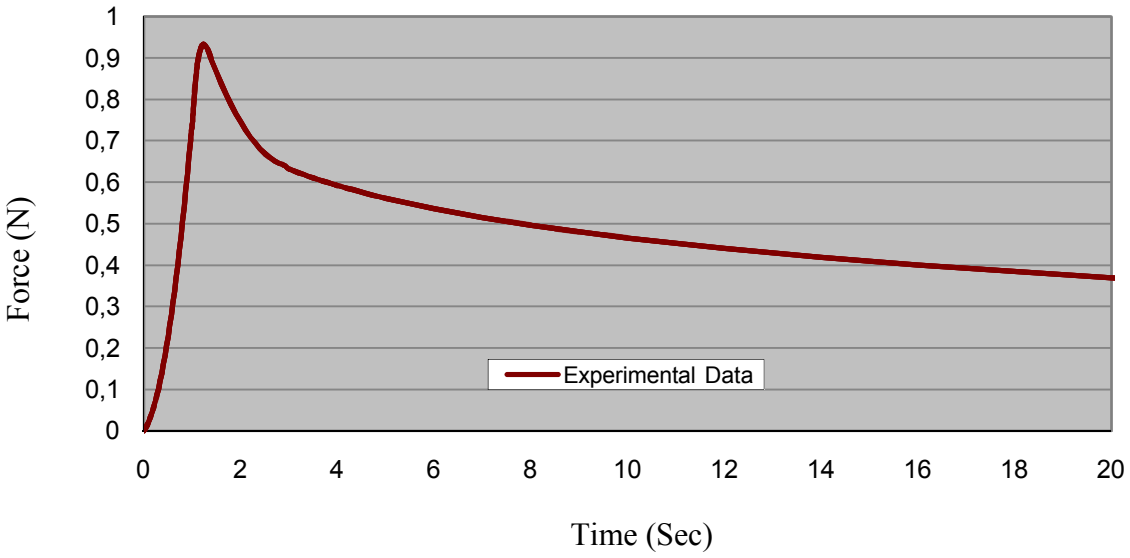

Figure 6.6 Filtered Smooth Experimental Data

6.3 Optimization Results

For optimization, force reaction graph must be optimized to experimental force reaction graph. The process was explained in optimization chapter. After completing the optimization we get new material coefficients from ANSYS. With this optimized material coefficients, a new FEA model is created.

Input Parameter Goals

Name	Lower Bound	Upper Bound
C01	2.3e-003	3.5e-003
C10	3.2547e-003	3.5973e-003
T1	0.9	1.1
T2	5.	9.
A1	0.38	0.4323
A2	0.2394	0.28

Parameter	Candidate A	Candidate B	Candidate C
C01	2.0809e-003	2.1124e-003	2.0431e-003
C10	3.5603e-003	3.4443e-003	3.6737e-003
T1	1.2891	1.1706	1.2698
T2	9.6467	9.8817	8.679
A1	0.30243	0.30892	0.32742
A2	0.20666	0.2168	0.21883
RF	7.572e-002 ★★★	0.11141 ★★★	0.12672 ★★★

The most positive rating of ★★★ means that the design is excellent in terms of satisfying the goal defined for the parameter.

Figure 6.7 Input Parameters and Candidate (optimized) Parameters Taken from ANSYS

Figure 6.7 is the coefficients for tested material with indenter depth of 6 mm and the candidates with lower RF (square error function) must be selected as material model coefficients. As seen in figure three star rating is the excellent rating and it is satisfying the goal defined for the material.

6.3.1 Material Coefficients

As discussed above, stress relaxation tests have been applied upon materials with different viscoelastic structures. At the end of these, material coefficients have been compared within for a specific depth of 6mm.

In Table 6.1, material coefficients for different materials can be seen. C01 and C10 are hyperelastic (Mooney Rivlin); T1, T2, A1 and A2 are viscoelastic (Prony Series) coefficients.

Table 6.1 Material Coefficients

Tests	Initial Values	Test 1 Gel 6mm Optimization	Test 2 Arm 6mm Optimization	Test 3 Foam 6mm Optimization
Material	Pig Liver	Viscoelastic Gel	Soft Tissue	Viscoelastic Foam
Depth	-	6 mm	6 mm	6 mm
C01 (kPa)	0.003426	0.002317	0.00208	0.00109
C10 (kPa)	0.003426	0.00266	0.00356	0.00376
T1 (s)	1.0	0.913	1.289	0.7317
T2 (s)	9.0	8.686	9.6467	9.6847
A1	0.393	0.4166	0.3024	0.39813
A2	0.266	0.243379	0.2066	0.16704
RF (N)	-	0.686	0.0075	0.10962

6.3.2 3D Graphs of Material Coefficients Respect to RF (Error)

Below are 3D graphs of the change material coefficients into RF (Error), after the optimization. The change among coefficients within the same model is observed in these graphs. Different model coefficients still have effects on each other, even if it is low. Minimum applied iteration of six material coefficients onto RF are taken into consideration, when optimizing. As declared by ANSYS, this iteration is applied via Golden Driven Optimization.

In order;

1) Hyperelastic material coefficient (Mooney Rivlin) – RF (Error) change of C10 and C01 (Figure 6.8)
2) Viscoelastic material coefficient (Prony Series) - RF (Error) change on T1 and T2 (Figure 6.9)
3) Viscoelastic material coefficient (Prony Series) - RF (error) change on A1 and A2 (Figure 6.10)
4) Change of T1 and A1 among themselves and according to RF (Figure 6.11)
5) Change of T2 and A2 among themselves and according to RF (Figure 6.12)

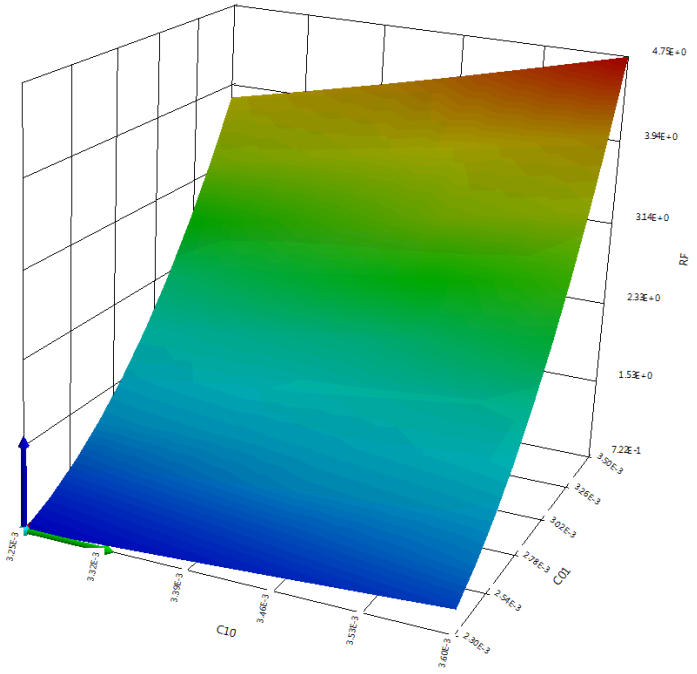

Figure 6.8 C10 and C01 Coefficients Respect to RF

As seen in the figure, the change in hyperelastic material coefficients of Mooney Rivlin, C10 and C01, affects RF. Increase in C01 has a larger effect on the increase of error, rather than increase in C10, resulting in a smooth error graph. This further shows that C01 is the dominant coefficient. Compared with other coefficients, change in these cause are larger and contains bigger errors. In other graphs, the error margin is around 1.4%, while with these coefficients the error margin becomes 4.7%. This is because one of the models in two model based simulation solely depends on these two coefficients, hence resulting in a dominant effect in the simulation

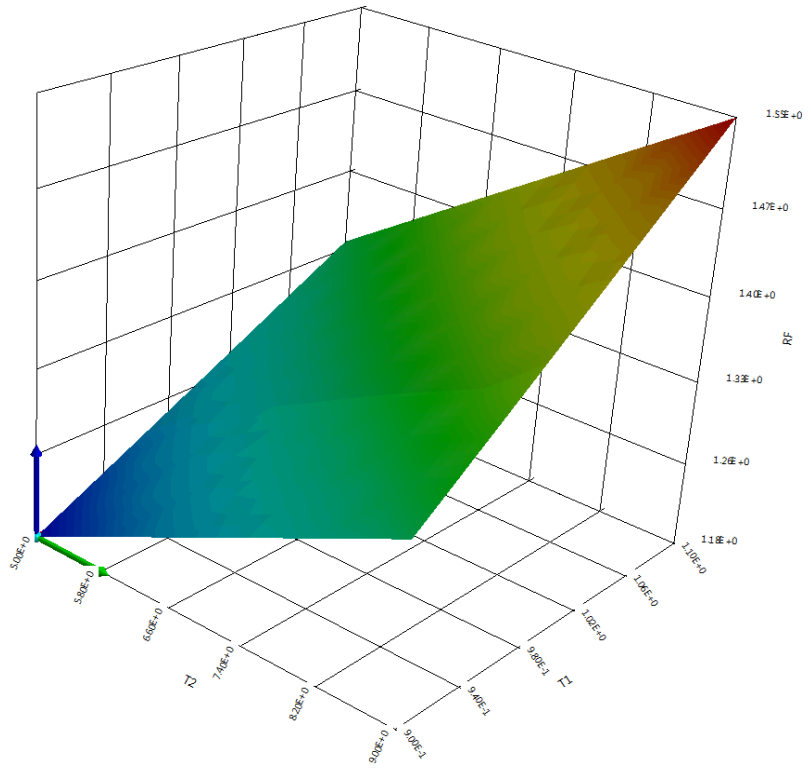

Figure 6.9 T1 and T2 Coefficients Respect to RF

In figure 6.9, the effect of T1 and T2, coefficients of Prony series, on the error is clearly observed. These coefficients define the relaxation time for each Prony component in Prony series. The ratio of change among T1 and T2 are very sensitive, showing that there are rapid spikes in rate of increase in error (Non-Smooth).

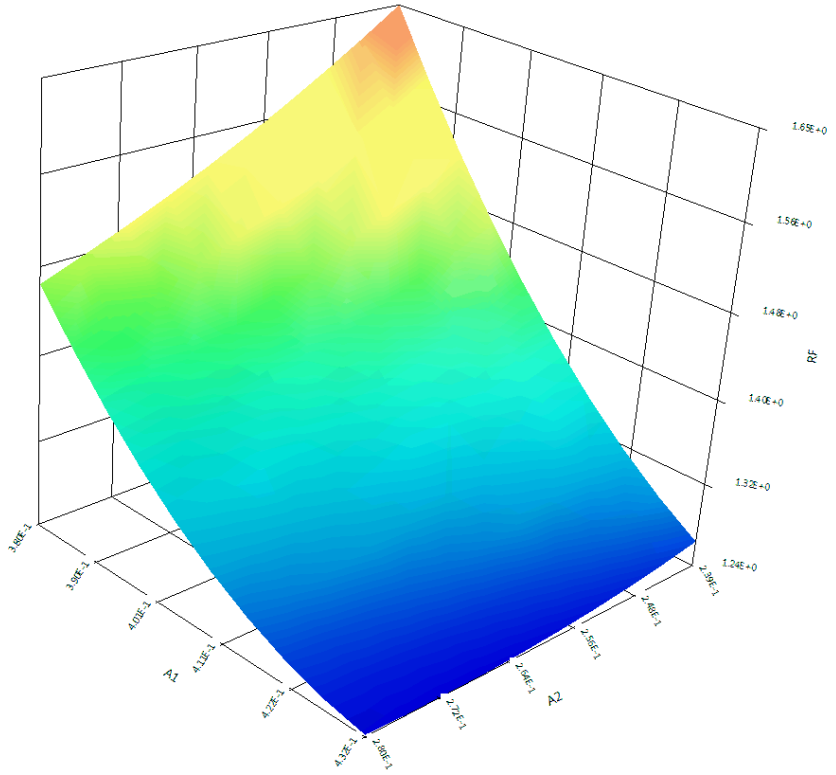

Figure 6.10 A1 and A2 Coefficients Respect to RF

Figure 6.10 is the graph concerning A1 and A2's error which are another two coefficients of Prony Series. These two are shear elastic/relative modules in Prony Series. The error transition between coefficient changes is rather smooth, hence influencing the error in a mediocre way.

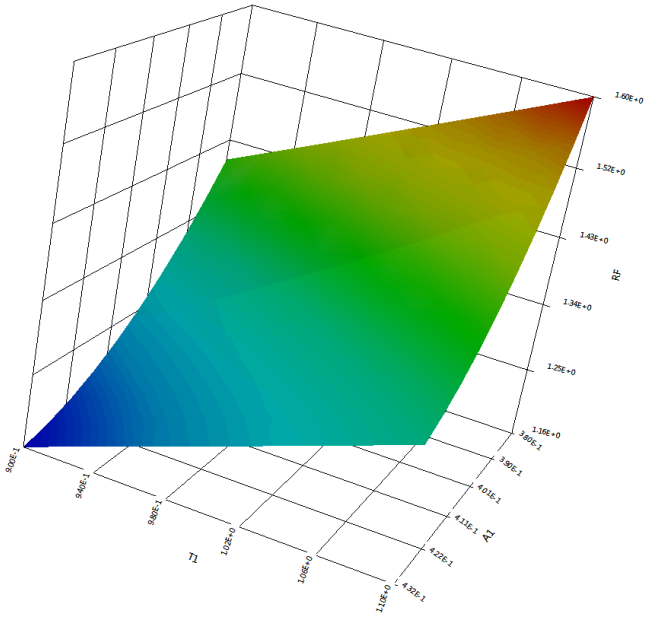

Figure 6.11 T1 and A1 Coefficients Respect to RF

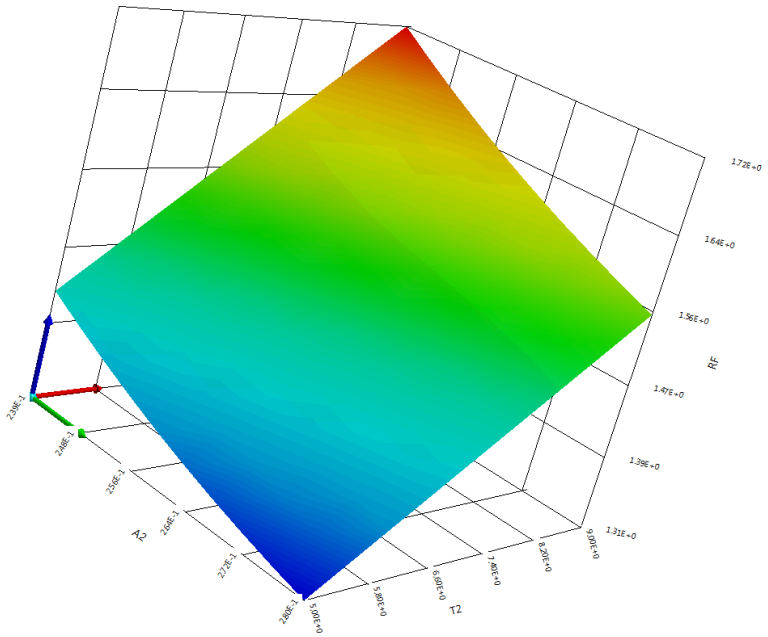

Figure 6.12 T2 and A2 Coefficients Respect to RF

Figure 6.11 and 6.12 shows the influence of T and A, two coefficients of Prony Series, on RF together. The relation between the coefficients T and A coefficients are rather weak and their changes according to each other result in rapid Error values.

6.4 Inverse Finite Element Solution with Optimized Values

With optimized material coefficients, a new model was created, resulting in the following graphs in order:

- Total deformation graph (Figure 6.13)
- Equivalent stress graph (Figure 6.14)
- Equivalent elastic strain graph (Figure 6.15)
- Maximum principal elastic strain graph (Figure 6.16)
- Force Reaction graph (Relaxation graph) (Figure 6.17)

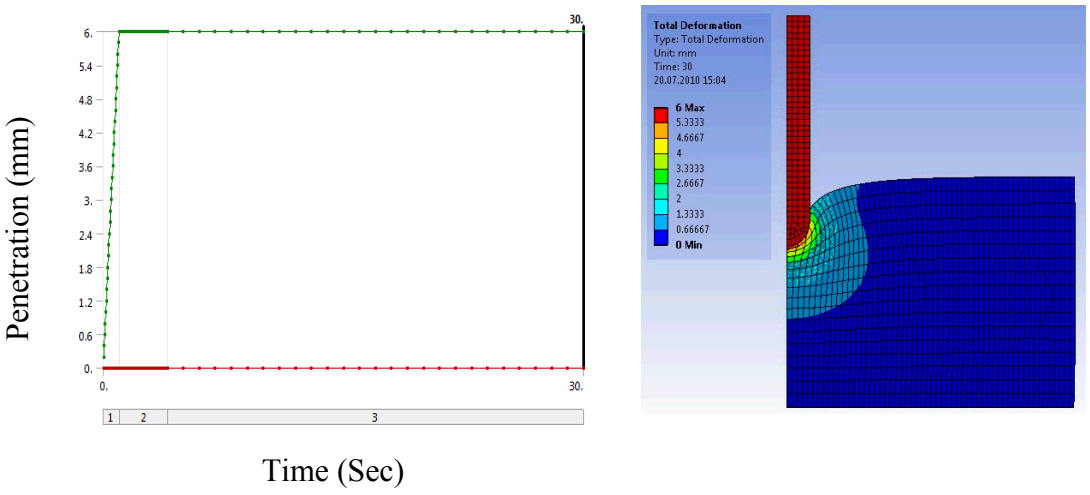

Figure 6.13 Penetration Graph and Simulation for Optimized Values

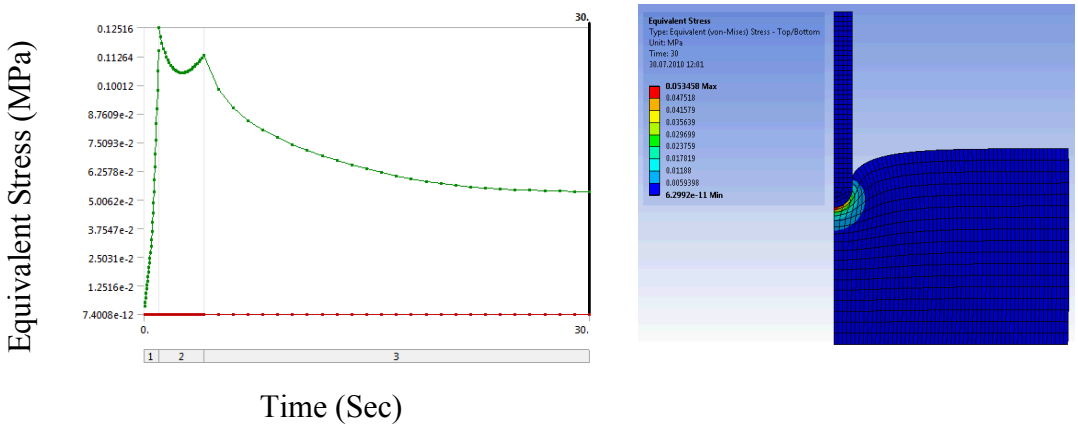

Figure 6.14 Equivalent Stress Graph and Simulation for Optimized Values

The Equivalent Stress values of the model are newly created, with optimized values and they are roughly 20 percent less than the initial model values. But this result did not produce a change in the smoothness of the graph as it was expected.

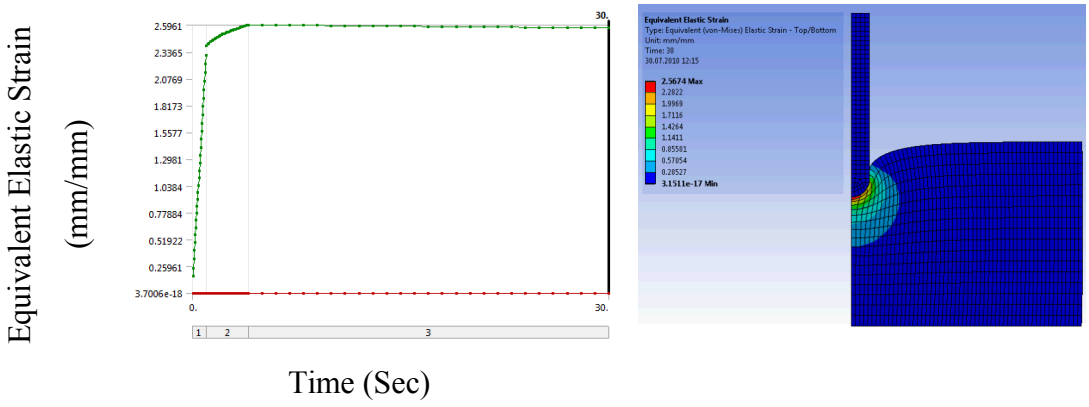

Figure 6.15 Equivalent Elastic Strain Graph and Simulation for Optimized Values

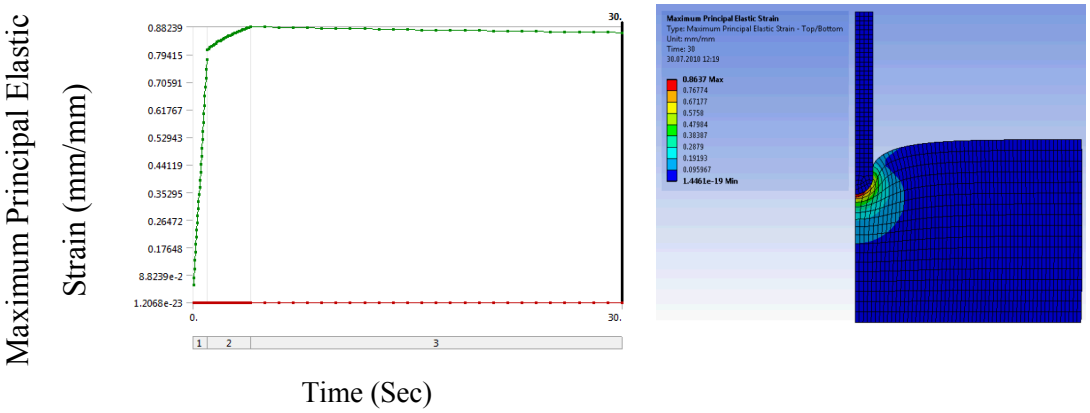

Figure 6.16 Maximum Principal Elastic Strain Graph and Simulation for Optimized Values

In terms of equivalent elastic strain and maximum principal elastic strain, an increased value is observed, compared with the initial model. There are no changes in the slopes of these graphs, only some increase in the graph values is observed.

Below is the Force Reaction (Relaxation) graph, according to newly calculated values. As expected, force Reactions have lower values, since the material tested has more viscoelastic structure than the initial material. Since the material is viscoelastic gel, its counter-force upon the identifier is lower and material is softer than the initial material.

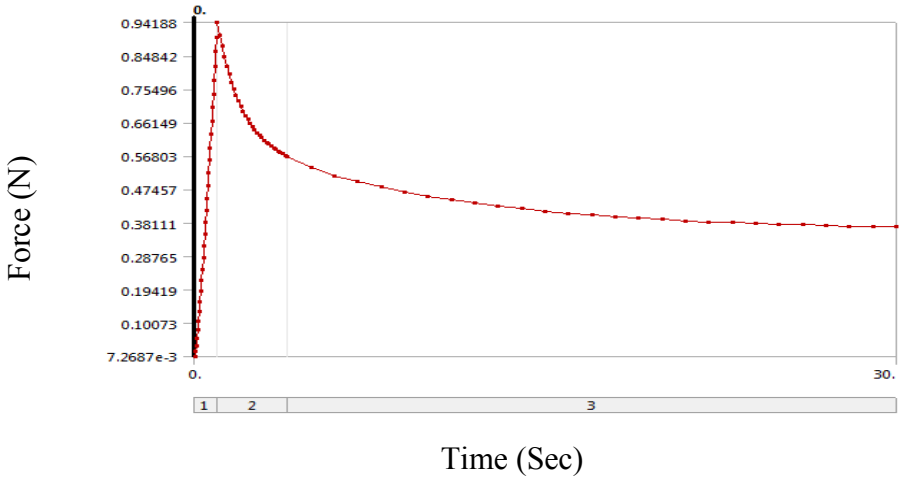

Figure 6.17 Force Reaction (Relaxation) Graph for Optimized Values

6.5 Comparison of Results

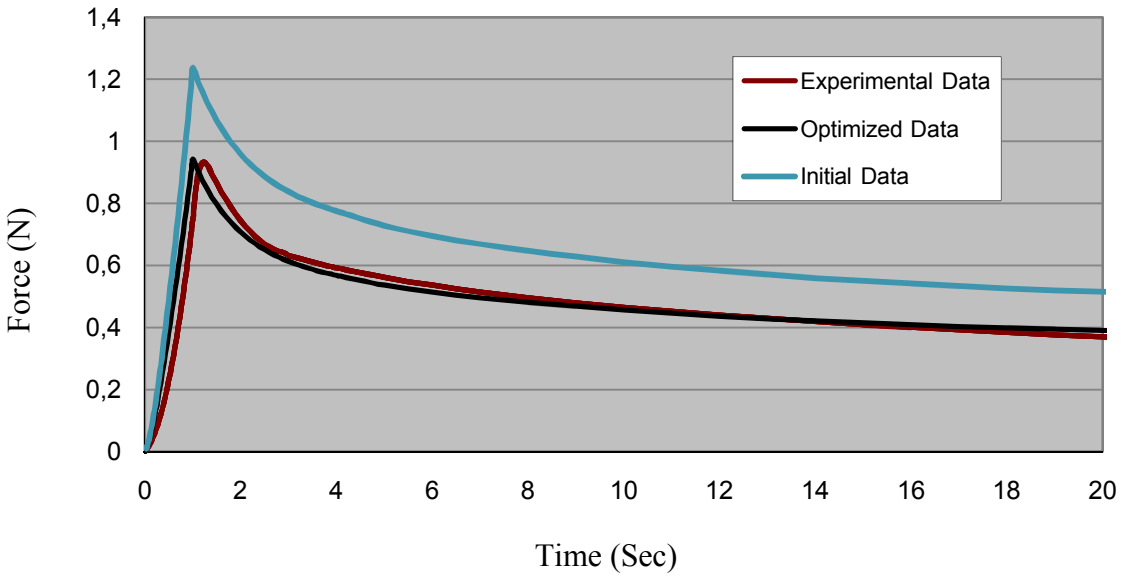

Figure 6.18 Optimization Result for Viscoelastic Gel w/ 6mm

In the graph Figure 6.18, blue sections represents the Force Reaction (Relaxation) graph of the model with initial values, brown one represents the stress relaxation data received from the experiments, and the black corresponds to the Force Reaction (Relaxation) graph of the optimized model. The values of material coefficients after the optimization process are very close to the values of the experiment, as it can be clearly seen. In compliance with previous statement, the RF value after optimization is very low, roughly around 0.0757N, which shows that the optimization of material model coefficients for viscoelastic gel according to stress relaxation test is successful.

As a result, the modeled material produces very close values compared with the tested viscoelastic gel material, which leads to the conclusion that material characteristics of tested material is correctly identified. In other words, tested viscoelastic gel material has been simulated with selected model in ANSYS according to stress relaxation test. This material is our example for examine and understand the process for FEA and optimization. As mentioned before all data and

graphs which are discussed in Result Chapter is taken from viscoelastic gel w/ 6mm penetration's finite element analysis and optimization process.

6.6 Optimization Results of Other Materials

In our study, we worked with different materials and different penetration ratios. In below section, discussion of these stress relaxation test result, optimization and optimized materials stress relaxation graphs can be found.

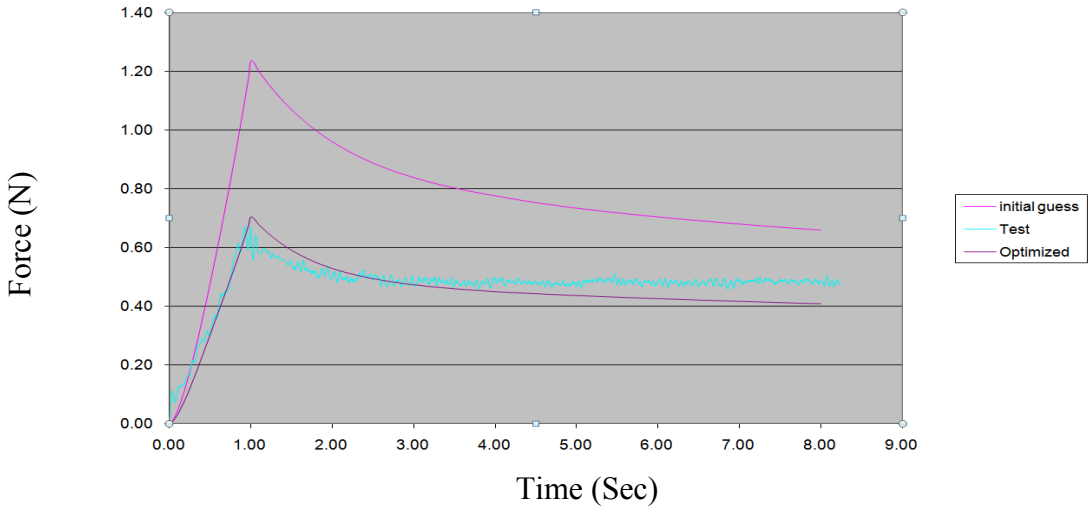

Figure 6.19 Optimization Result for Viscoelastic Foam w/ 6 mm

Our optimization process is also successful in viscoelastic foam with 6 mm penetration. In the graph Figure 6.19 the stress relaxation data of optimized model is very close to test data and the error (RF) value after optimization is very low. The maximum force value is lower than viscoelastic gel's material because of foam softness. In 6 mm penetration, maximum 0.7 N force value can be seen in graph. Instead of this, peak of force relaxation graph is smoother than gel material. It is related with material's behavior. By this way, we can conclude that our experimental setup can plot correct stress relaxation graphs according to materials properties & behavior and also our optimization is successful.

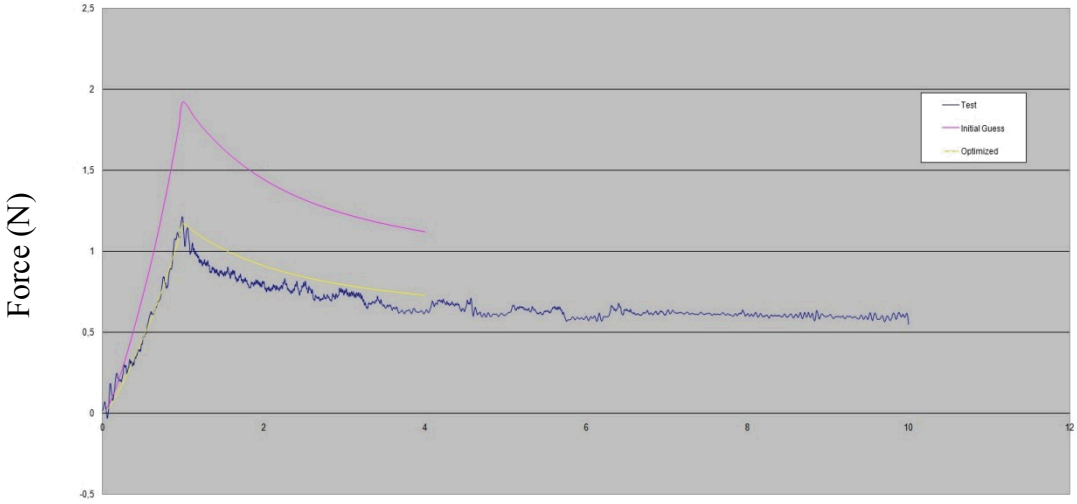

Figure 6.20 Optimization Result for Viscoelastic Foam w/ 8 mm

In Figure 6.20, different penetration depth (8 mm) is applied to viscoelastic material with experimental setup. The maximum force goes up to 1.2 N due to 8 mm penetration. The peak of stress relaxation is same with 6 mm penetration. Our optimization is acceptable and error (RF) value is low. We correctly simulate our model with viscoelastic foam material and 8 mm penetration depth according to stress relaxation test.

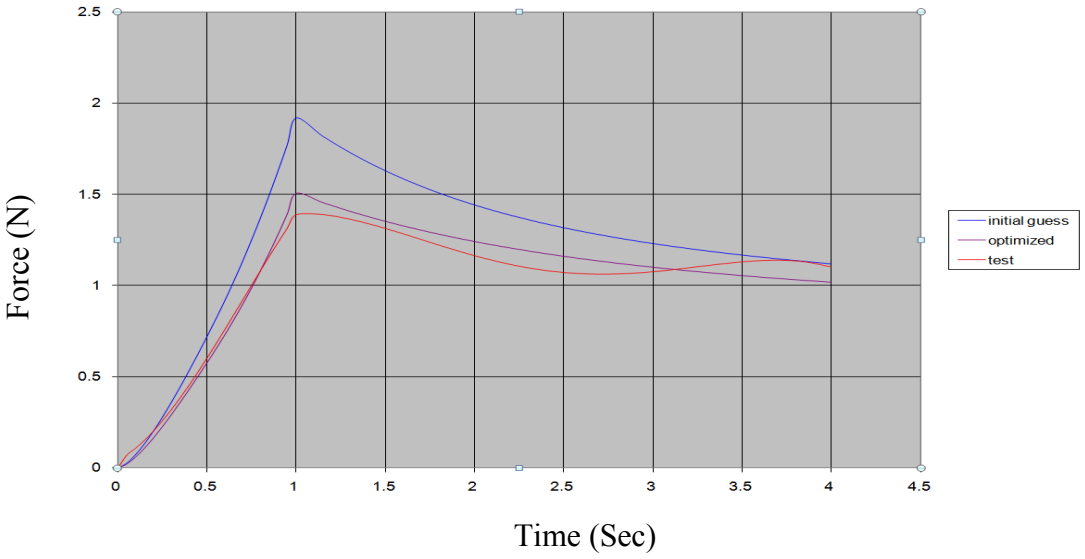

Figure 6.21 Optimization Result for Soft Tissue (Arm) w/ 8 mm

Soft tissue is very difficult material for test process (stress relaxation) and also for optimization. Because of the stability problem, small penetration depths such as 4 mm or 6 mm cannot give proper stress relaxation graphs. The data is affected from pulse, stability of arm and little movement of human being, so there are major noises in stress relaxation graph which our Low Pass Filter cannot filter it properly.

For this reason, 8 mm penetration depth is used in soft tissue experiments. Even 8 mm depth we still have noises which affect stress relaxation graph in indenter test method. It can be easily seen in Figure 6.21, after filtering raw data, stress relaxation graph has still some undulation. And the error value is approximately 0.1 N which is higher than other optimization errors because of this undulation. For this case, we optimized model coefficients and created a new optimized model. But optimization values and error are not successful as other materials. In other word, optimized model does not completely represent soft tissue in simulation of ANSYS.

CHAPTER 6

CONCLUSION

In this study, the main purpose is simulating of tested materials by using finite element analysis method with proper models and their coefficients. In order to achieve this objective, many stress relaxation tests with viscoelastic materials (gel, viscoelastic foam and soft tissue – arm) were performed by using the prepared experimental setup.

By using the haptic based experimental setup, many stress relaxation tests were conducted upon gel, viscoelastic foam and the soft tissue of a human forearm. Different penetration depths have been applied (4,6,8 mm) to the different materials in order to get different stress relaxation graphs. 6 and 8 mm penetration and their stress relaxation graphs were used to obtain the optimized materials coefficients. It was observed from the experiments that 4 mm penetration depth is not suitable for gel and foam viscoelastic materials since experimental setup cannot obtain proper data of stress relaxation according to their material softness. At least 6 mm penetration depth is needed for viscoelastic foam and gel. On the other hand, minimum penetration depth for soft tissue (forearm) is 8 mm for the same reason.

Stress relaxation test has been simulated by using finite element analysis method with initial data. This work has also been conducted via an indenter/experimental test setup.

Another objective of this study is optimization of model coefficients of the tested materials with suitable optimization method. Data acquired from FEA has been optimized with respect to the data acquired from the experiment. After this optimization, material coefficients of the tested material are calculated.

After completing optimization studies, an acceptable error range between 0.06 N and 0.08 N for viscoelastic foam and gel with penetration depth 6 and 8 mm were found. It is proven that applied optimization is accurate and acceptable. In other words, finite element model with optimized coefficients is successfully simulated the tested material according to stress relaxation graph.

Due to the stability problems during the experiment process, soft tissue (forearm) error values goes up to ≈ 0.1 N. Force sensor used in our experimental setup is very sensitive (sensing rate range ±50 N and resolution 1/160 N). Little movement of arm, pulse and fixing problems of arm give us stress relaxation graph with very noisy force data. After filtering noisy data, still we have undulation on stress relaxation graph. For this reason it can be said that optimization error value of arm (soft tissue) is greater than other viscoelastic materials.

Model of tested material and its justification and the experimentally identified suitable model coefficients are achieved by initially determining a suitable material model and their coefficients obtained from inverse finite analysis. Two Term Mooney Rivlin method for hyperelastic behavior and Prony Series method for viscoelastic behavior have been used in this model. In total six material coefficients are present for model identification; two for Mooney Rivlin (C01,C10 – Material stiffness constants) and four for Prony Series (A1,A2 – Relative modili & T1,T2 – Relaxation times).

Stress relaxation data of gel material with 6 mm penetration have been chosen for illustration in the study. Since, error value of optimization in viscoelastic gel is minimum (0.0057 N). Therefore, it is the best optimized material according to stress

relaxation data. The effects of the optimized coefficients to the error can be indicated as follows:

Mooney Rivlin coefficients show that C01 is dominant material coefficients during the optimization, according to RF graph, and it influences error up to 4.7%.

On the other hand, Prony Series coefficients T1 and T2 influence the error in a smoother way. The change in these two coefficients gives a maximum 1.6% change in error. Also A1 and A2 influence the error in a small change (less than 1%).

Tested material has been modeled with its optimized coefficients at the last step. The experiment process has been re-simulated in FEA and its stress relaxation data has been acquired for comparison.

It is observed that the stress relaxation graphs obtained from the FEA and experiments are very close. The identification of tested materials characteristics for selected models has been accurate for stress relaxation test. It can be concluded that the tested material is successfully simulated /modeled for selected material models in ANSYS with the help of stress relaxation data.

As stated, we have two main contributions in this study. First one is; experimental setup with user-friendly graphical user interface (GUI) provides user to change/adjust path of indenter, PID values and plot graphs. By the same manner, other test methods can be performed for various viscoelastic materials. The other contribution is optimizing other suitable viscoelastic materials coefficients by using our ANSYS algorithm with stress relaxation data.

For future work, haptic rendering will be added to interface and GUI. Completely haptic rendered material via help of FEA can be simulated and proper experiments can be done for the selected material with experimental setup. Also other test methods such as static and cyclic loading, creep test, etc. can be done with our

experimental setup. The simulation and optimization of model coefficients studies can be done in ANSYS with similar processes.

REFERENCES

[1] Samur E., Sedef M., Basdogan C., Avtan L., Duzgun O., 2007. A robotic indenter for minimally invasive measurement and characterization of soft tissue response, 361-373.

[2] Liu G. R., Quek S. S., 2003. The Finite Element Method A Practical Course. London.

[3] Fung Y. C., 1993. Biomechanics: Mechanical Properties of Living Tissues, 2nd ed., Springer-Verlag.

[4] Kwan K. H., 1985. Static and cyclic behaviors of multistory infilled frames with different interface conditions. J. Sound Vibr., 275–283.

[5] Svecova Z., Cuth V., Slabeycius, J., Kopecky M., 2005. Evaluating of Hyperelastic Material Behavior.

[6] Sedef M., Samur E., Basdogan C., 2006. Visual and Haptic Simulation of Linear Viscoelastic Tissue Behavior Based on Experimental Data, 58-68.

[7] Meyers M. A., Chawla K.K., 2006. Mechanical Behavior of Materials. Prentice Hall, US edition.

[8] Knudson D., 2007. Fundamentals of Biomechanics. Springer Science, 2nd ed., New York.

[9] Zeng Y., Yang J., Huang K., Lee Z., Lee X., 2001. A comparison of biomechanical properties between human and porcine cornea, 533-537.

[10] Fung Y. C., Tong P., 2001. Classical and Computational Solid Mechanics, Volume 1, Advanced Series in Engineering Science.

[11] Roylance D., 2001. Report, Department of Material Science and Engineering, Massachusetts Institute of Technology, Cambridge.

[12] Kaliske M., Rothert H., 1997. Formulation and Implementation of Three-Dimensional Viscoelasticity at Small and Finite Strains, Computational Mechanics, vol. 19, pp. 228-239.

[13] Elliott R.P., 1965. Constitution of Binary Alloys, I-Supplement. McGraw-Hill Book Co., Inc., New York, USA

[14] Fung, Y. C., Sobin S.S., 1972. Elasticity of the pulmonary alveolar sheet, 451-469.

[15] Danielson D A, 1973. Human Skin as an Elastic Membrane. Elsevier Science, Vol.6, pp.539-546.

[16] Fung Y .C., 1965. Foundations of Solid Mechanics, Prentice-Hall, New Jersey.

[17] Gefen A., Margulies S. S., 2003. Are in vivo and in situ brain tissues mechanically similar, Journal of Biomechanics 37, 1339-1352.

[18] Tanaka E., Tanaka M., Aoyamaa J., Watanabe M., Hattori Y., Asai D., Iwabea T., Sasaki A., Sugiyama M., Tane K., 2002. Viscoelastic properties and residual strain in a tensile creep test on bovine temporomandibular articular. Archives of Oral Biology 47, 139–146.

[19] Yin Y., Ling S., Liu Y., 2004. A dynamic indentation method for characterizing soft incompressible viscoelastic materials. Materials Science and Engineering 379, 334-340.

[20] Rognes Marie E., 2005. Mixed Finite Element Methods for Elasticity and Viscoelasticity, University of Oslo, Oslo.

[21] Balmforth N.J., Craster R.V., 2001. Geophysical Aspects of Non-Newtonian Fluid Mechanics.

[22] Başer Ö., 2006. Haptic Device Design. M. Sc. Thesis, Middle East Technical University. Ankara, Turkey.

[23] ANSYS 11.0, 2005. Help & Tutorials. http://www.kxcad.net/ansys/ANSYS/ansyshelp/Hlp_UI_Tutorials.html.

[24] ANSYS 11.0, 2004. Theory Reference for ANSYS and ANSYS Workbench. Ansys Relase 9.0, Canonsburg, PA.

[25] Petekkaya A. T., 2008. In Vivo Experiments on Soft Biological Tissues for Identification of Materials Models and Corresponding Parameters, M. Sc Thesis, Middle East Technical University. Ankara, Turkey.